

Resolvent-Type Data-Driven Learning of Generators for Unknown Continuous-Time Dynamical Systems

Yiming Meng*, Ruikun Zhou*, Melkior Ornik, *Senior Member, IEEE*, and Jun Liu, *Senior Member, IEEE*

Abstract—A semigroup characterization, or equivalently, a characterization by the generator, is a classical technique used to describe continuous-time nonlinear dynamical systems. In the realm of data-driven learning for an unknown nonlinear system, one must estimate the generator of the semigroup of the system’s transfer operators (also known as the semigroup of Koopman operators) based on discrete-time observations and verify convergence to the true generator in an appropriate sense. As the generator encodes essential transient transitional information of the system, challenges arise for some existing methods that rely on accurately estimating the time derivatives of the state with constraints on the observation rate. Recent literature develops a technique that avoids the use of time derivatives by employing the logarithm of a Koopman operator. However, the validity of this method has been demonstrated only within a restrictive function space and requires knowledge of the operator’s spectral properties. In this paper, we propose a resolvent-type method for learning the system generator to relax the requirements on the observation frequency and overcome the constraints of taking operator logarithms. We also provide numerical examples to demonstrate its effectiveness in applications of system identification and constructing Lyapunov functions.

Index Terms—Unknown nonlinear systems, infinitesimal generator, operator-logarithm-free, observation sampling rate, convergence analysis.

I. INTRODUCTION

OPERATOR semigroups are essential for characterizing Markov processes, whether random or deterministic. In the scope of the approximation a Markov process, the convergence of an approximating sequence of processes should be studied. The technique involves studying the convergence of the processes’ (infinitesimal) generators in an appropriate sense. Such convergence implies the convergence of the processes’ transition semigroups, which, in turn, implies the convergence of the processes to the true Markov process [1].

For a continuous-time nonlinear dynamical system, the operator semigroup, denoted by $\{\mathcal{K}_t\}_{t \geq 0}$, is known as the

This research was supported in part by NASA under grant numbers 80NSSC21K1030 and 80NSSC22M0070, by the Air Force Office of Scientific Research under grant number FA9550-23-1-0131, and in part by the Natural Sciences and Engineering Research Council of Canada and the Canada Research Chairs program.

*Equal contribution.

Yiming Meng is with the Coordinated Science Laboratory, University of Illinois Urbana-Champaign, Urbana, IL 61801, USA. yymmeng@illinois.edu.

Ruikun Zhou is with the Department of Applied Mathematics, University of Waterloo, Waterloo ON N2L 3G1, Canada ruikun.zhou@uwaterloo.ca.

Melkior Ornik is with the Department of Aerospace Engineering and the Coordinated Science Laboratory, University of Illinois Urbana-Champaign, Urbana, IL 61801, USA. mornik@illinois.edu.

Jun Liu is with the Department of Applied Mathematics, University of Waterloo, Waterloo ON N2L 3G1, Canada j.liu@uwaterloo.ca.

semigroup of transfer operators, which are also called Koopman operators [2]. The corresponding infinitesimal generator, \mathcal{L} , is a differential operator (most likely unbounded [3, Chapter VIII]) that provides essential transient transitional information for the dynamical system [4]. Particularly, many mass transport-related PDEs, such as transport equations [5], Lyapunov equations [6], and Hamilton-Jacobi equations [7]–[9], are defined by the generator. Their solutions serve as valuable tools for discovering physical laws [10], [11] and verifying dynamical system properties related to stability [12]–[14], safety [15]–[17], and kinetic and potential energy [4], [5], with applications across various fields including mechanical, space, and power systems, as well as other physical sciences.

To learn unknown continuous-time dynamical systems, one must approximate the entire semigroup, or equivalently its generator, from discrete trajectory data and demonstrate convergence to the true system in an appropriate sense. Considering possible nonlinear effects, challenges arise in retrieving transient system transitions from unavoidable discrete-time observations. Particularly in real-world applications, due to the limitations of sensing apparatuses in achieving high-frequency observations, it is difficult to accurately evaluate quantities related to transient transitions, such as those involving time derivatives.

To enhance learning accuracy, we aim to propose a Koopman-based generator learning scheme that relaxes the observation rate compared to existing methods and demonstrates its convergence to the true generator. Below, we review some crucial results from the literature that are pertinent to the work presented in this paper.

A. Related Work

The equivalence between the vector field and the infinitesimal generator of the system semigroup has been shown in [2], [18], indicating an equivalence in terms of conventional system (model) identification and generator (or semigroup) characterization.

For autonomous dynamical systems, direct methods such as Bayesian approaches [19] and the sparse identification of non-linear dynamics (SINDy) algorithm [20] have been developed to identify state dynamics with a known structure [10], [11], relying on nonlinear parameter estimation [21], [22] and static linear regression techniques. However, direct methods require that time derivatives of the state can be accurately estimated, an assumption that may not be robustly satisfied due to potential challenges such as low sampling rates, noisy measurements, and short observation periods.

Indirect characterization methods can leverage the learning structure of Koopman operators [23]. By applying certain transformations to the learned Koopman operator, the image of the generator related to the transient state dynamics can be expressed as a linear combination of dictionary functions. Such a framework is based solely on observed state data snapshots, which enhances the robustness of characterization through linear least squares optimization over an expressive dictionary that includes nonlinear functions. An additional benefit of using indirect methods is that they can streamline the procedures for generator characterization and solving transport-related PDEs using the same set of dictionary functions, including neural network bases [24]–[27]. In this introduction, we summarize two widely used Koopman-based characterization methods.

Finite-difference method (FDM) is a numerical technique used to solve differential equations by approximating derivatives with finite differences. In the context of Koopman-based learning, the generator on any observable function is approximated by the rate of its evolution along the trajectory, using a forward difference method with a small discretized time scale. Similar to direct methods, this approximation scheme also relies on the notion of evolution speed or time derivatives. As anticipated, its precision heavily depends on the size of the temporal discretization [28]–[32].

Recent studies [29], [33]–[35] have facilitated another indirect learning of the generator using the logarithm of the learned Koopman operator. This approach can potentially circumvent the need for high observation rates and longer observation periods, as it does not require the estimation of time derivatives. Heuristically, researchers tend to represent the Koopman operator \mathcal{K}_t by an exponential form of its generator \mathcal{L} as $\mathcal{K}_t = e^{t\mathcal{L}}$, leading to the converse representation $\mathcal{L} = \frac{1}{t} \log(\mathcal{K}_t)$ for any $t > 0$. However, problems arise given the following concerns: 1) representing Koopman operators in exponential form requires the boundedness of the generator \mathcal{L} ; 2) the operator logarithm is a single-valued mapping only within a specific sector of the spectrum; 3) for general systems that fall short of the aforementioned restrictions, it is unclear how the data-driven approximation of the logarithm of Koopman operators converges to the true generator.

As a complement to the work in [33], [34], recent studies [36], [37] have rigorously investigated the sufficient and necessary conditions under which the Koopman-logarithm based generator learning method can guarantee learning accuracy. To provide the sampling rate, the theorem relies on the concept of a “generator-bounded space”, which remains invariant under the Koopman operator, and where the generator is bounded when restricted to it. However, the mentioned concept is less likely to be verifiable for unknown systems.

B. Contributions

To address the aforementioned issues, we aim to propose an operator logarithm-free generator learning scheme, named the *resolvent-type method* (RTM), which is robust to the choice of the dictionary of observable functions and does not require knowledge of spectral properties of the Koopman operators.

A brief discussion on the resolvent of the Koopman generator can be found in [38]. However, to the best of the authors’ knowledge, the current work is the first to utilize a resolvent-based method to identify the generator and, consequently, the vector fields. In summary, the main contributions are:

- 1) We demonstrate the converse relationship between the Koopman operators and the generator in more general cases where the generator may be unbounded. Specifically, we draw upon the rich literature to propose a finite-dimensional approximation based on Yosida’s approximation for these cases.
- 2) We provide the analytical convergence rate of this approximation and demonstrate the theoretical feasibility of a data-driven adaptation.
- 3) We adapt the Koopman operator learning structure for generator learning based on 1), and demonstrate that a modification is needed to accommodate a low observation rate constraint.
- 4) We provide numerical experiments and demonstrate the effectiveness of the proposed approach by comparing it with the FDM and logarithm-based methods.

Notice of Previous Publication. This manuscript substantially improves the work of [39] in the following aspects: 1) All key convergence proofs are completed, providing step-by-step reasoning on the development of the proposed method; 2) The key step of the learning algorithm is provided, explicitly demonstrating the dependence on tuning parameters; 3) A novel modification is derived to relax the constraint on the observation rate; 4) Numerical simulations on representative systems are thoroughly studied.

The rest of the paper is organized as follows. In Section II, we present some preliminaries on dynamical systems and the corresponding semigroup, and revisit the basic concept of operator convergence. In Section III, we provide a Yosida-type approximation for the infinitesimal generator in the strong operator topology and explicitly show the analytical convergence rate, which will foster a better understanding for the development of data-driven approximations. In Section IV, we verify the feasibility of using a data-driven approximation by providing a finite-horizon, finite-dimensional reduction based on the analysis in Section III. The data-driven algorithm is provided in Section V. In particular, we show that a modification can be made to the proposed resolvent-type method to accommodate a low observation rate. We provide numerical simulations in Section VI to demonstrate the performance of the proposed method.

C. Notation

We denote by \mathbb{R}^d the Euclidean space of dimension $d > 1$, and by \mathbb{R} the set of real numbers. We use $|\cdot|$ to denote the Euclidean norm. For a set $A \subseteq \mathbb{R}^d$, \bar{A} denotes its closure, $\text{int}(A)$ denotes its interior and ∂A denotes its boundary. We use the Frobenius norm $\|\cdot\|_F$ as the metric for finite-dimensional matrices. We also use \cdot^T and \cdot^\dagger to denote the matrix/vector transpose and pseudoinverse, respectively.

For any complete normed function space $(\mathcal{F}, \|\cdot\|_{\mathcal{F}})$ of the real-valued observable functions, and for any bounded linear

operator $\mathcal{B} : \mathcal{F} \rightarrow \mathcal{F}$, we define the operator (uniform) norm as $\|\mathcal{B}\| := \sup_{\|h\|_{\mathcal{F}}=1} \|\mathcal{B}h\|_{\mathcal{F}}$. We denote by Id the identity operator on any properly defined spaces. Let $\mathcal{C}(\Omega)$ be the set of continuous functions with domain Ω . We denote the set of i -times continuously differentiable functions by $\mathcal{C}^i(\Omega)$.

For the reader's convenience, we also provide a partial list of notations related to the technical details, which will be explained later in the article.

- M : the number of sampled initial conditions;
- N : the number of dictionary observable test functions;
- $\mathcal{Z}_N(x)$: the dictionary of N observable test functions;
- $\mathcal{K}_t, \mathcal{L}$: the Koopman operator and infinitesimal generator;
- K, L : the matrix version of a \mathcal{K}_t (with a fixed t) and the \mathcal{L} after data fitting, with dimension $N \times N$;
- τ_s : terminal observation instance for data collection;
- T_s : running time for performance verification;
- γ : observation/sampling frequency;
- Γ : number of snapshots for each trajectory during data collection, which is equal to $\gamma\tau_s$;
- τ : the sampling period, which is equal to $1/\gamma$.

From Section IV to VI, we will frequently use notations that represent approximations of certain quantities. We use $Q_{\text{sub}}^{\text{sup}}$ to denote an approximation of quantity Q that depends specifically on parameters appearing in the subscripts and superscripts, and use \tilde{Q} to denote an approximation of quantity Q without emphasizing its dependent parameters.

II. PRELIMINARIES

A. Dynamical Systems

Given a pre-compact state space $\Omega \subseteq \mathbb{R}^d$, we consider a continuous-time nonlinear dynamical system of the form

$$\dot{x} = f(x), \quad (1)$$

where the vector field $f : \Omega \rightarrow \Omega$ is assumed to be locally Lipschitz continuous.

Given an initial condition x_0 , on the maximal interval of existence $I \subseteq [0, \infty)$, the unique forward flow map (solution map) $\phi : I \times \Omega \rightarrow \Omega$ should satisfy 1) $\partial_t(\phi(t, x_0)) = f(\phi(t, x_0))$, 2) $\phi(0, x_0) = x_0$, and 3) $\phi(s, \phi(t, x_0)) = \phi(t + s, x_0)$ for all $t, s \in I$ such that $t + s \in I$.

Throughout the paper, we will assume that the maximal interval of existence of the flow map to the initial value problem (1) is $I = [0, \infty)$.

Remark 2.1: The above assumption is equivalent to assuming that the system exhibits forward invariance w.r.t. the set Ω . However, this is usually not the case for general nonlinear systems. In this paper, if the system dynamics violate the above assumption, we can adopt the approach outlined in [27, Section III.B] to recast the dynamics within the set $\tilde{\Omega}$. In other words, we constrain the vector field f such that $f(x) = 0$ for any $x \in \partial\Omega$, while f remains unchanged within the open domain Ω . This modification ensures that the system data is always collectible within $\tilde{\Omega}$. \diamond

B. Koopman Operators and the Infinitesimal Generator

Let us now consider a complete normed function space $(\mathcal{F}, \|\cdot\|_{\mathcal{F}})$ of the real-valued observable functions¹ $h : \Omega \rightarrow \mathbb{R}$.

Definition 2.2: A one-parameter family $\{\mathcal{S}_t\}_{t \geq 0}$ of bounded linear operators from \mathcal{F} into \mathcal{F} is a semigroup if

- 1) $\mathcal{S}_0 = \text{Id}$;
- 2) $\mathcal{S}_t \circ \mathcal{S}_s = \mathcal{S}_{t+s}$ for every $t, s \geq 0$.

In addition, a semigroup $\{\mathcal{S}_t\}_{t \geq 0}$ is a \mathcal{C}_0 -semigroup if $\lim_{t \downarrow 0} \mathcal{S}_t h = h$ for all $h \in \mathcal{F}$, and moreover a \mathcal{C}_0 -semigroup of contractions if $\|\mathcal{S}_t\| \leq 1$ for $t \geq 0$.

The (infinitesimal) generator \mathcal{A} of $\{\mathcal{S}_t\}_{t \geq 0}$ is defined by

$$\mathcal{A}h(x) := \lim_{t \downarrow 0} \frac{\mathcal{S}_t h(x) - h(x)}{t}, \quad (2)$$

where the observable functions are within the domain of \mathcal{A} , defined as $\text{dom}(\mathcal{A}) = \{h \in \mathcal{F} : \lim_{t \downarrow 0} \frac{\mathcal{S}_t h - h}{t} \text{ exists}\}$. \diamond

It is a well-known result that $\text{dom}(\mathcal{A}) = \mathcal{F}$.

The evolution of observables of system (1) restricted to \mathcal{F} is governed by the family of Koopman operators, as defined below. Koopman operators also form a linear \mathcal{C}_0 -semigroup, allowing us to study nonlinear dynamics through the infinite-dimensional lifted space of observable functions, which exhibit linear dynamics.

Definition 2.3: The Koopman operator family $\{\mathcal{K}_t\}_{t \geq 0}$ of system (1) is a collection of maps $\mathcal{K}_t : \mathcal{F} \rightarrow \mathcal{F}$ defined by

$$\mathcal{K}_t h = h \circ \phi(t, \cdot), \quad h \in \mathcal{F} \quad (3)$$

for each $t \geq 0$, where \circ is the composition operator. The (infinitesimal) generator \mathcal{L} of $\{\mathcal{K}_t\}_{t \geq 0}$ is defined accordingly as in (2). \diamond

Due to the (local) Lipschitz continuity of f in (1), and considering that observable functions are usually continuous, we will focus on $\mathcal{K}_t : \mathcal{C}(\Omega) \rightarrow \mathcal{C}(\Omega)$ for the rest of the paper. Consequently [4], $\mathcal{L} : \mathcal{C}^1(\Omega) \rightarrow \mathcal{C}(\Omega)$. For all continuously differentiable observable functions, i.e., $h \in \mathcal{C}^1(\Omega)$, the generator of the Koopman operators is given by

$$\mathcal{L}h(x) = \nabla h(x) \cdot f(x). \quad (4)$$

The space \mathcal{F} can be extended to $L^\infty(\Omega)$, which allows us to study the L^2 -adjoint operator of \mathcal{L} with domain $L^1(\Omega)$, leading to more interesting applications such as the Liouville equation and ergodic measure [4]. We will pursue generator learning on this extended domain in future work.

Remark 2.4: In view of Koopman-based indirect approximation of the generator, for each $h \in \mathcal{C}^1(\Omega)$, we have $\mathcal{K}_\tau h(x) - h(x) = \int_0^\tau \mathcal{L}h(\phi(s, x)) ds \approx \int_0^\tau \mathcal{L}h(\phi(0, x)) ds = \mathcal{L}h(x)\tau$, where the approximation is achieved through a small terminal time τ . Then, the derivative (of any h) along the trajectory is approximated by $\mathcal{L}h(x) \approx \frac{\mathcal{K}_\tau h(x) - h(x)}{\tau}$. Note that the finite-difference method (FDM) $\mathcal{L} \approx \frac{\mathcal{K}_\tau - \text{Id}}{\tau}$ simply follows (2) for sufficiently small $\tau > 0$. Through this approximation scheme of the time derivative, it can be anticipated that the precision heavily depends on the size of τ [28], [30], [31]. We will revisit the FDM in the numerical examples to compare it with the method proposed in this paper. \diamond

¹We clarify that in the context of operator learning, the term ‘‘observable functions,’’ or simply ‘‘observables,’’ commonly refers to ‘‘test functions’’ for operators, rather than to the concept of ‘‘observability’’ in control systems.

C. Representation of Semigroups

In this subsection, we introduce basic operator topologies and explore how a semigroup $\{\mathcal{S}_t\}_{t \geq 0}$ can be represented through its generator \mathcal{A} .

Definition 2.5 (Operator Topologies): Consider a Banach space $(\mathcal{F}, \|\cdot\|_{\mathcal{F}})$. Let $\mathcal{B} : \mathcal{F} \rightarrow \mathcal{F}$ and $\mathcal{B}_n : \mathcal{F} \rightarrow \mathcal{F}$, for each $n \in \mathbb{N}$, be linear operators.

- 1) The sequence $\{\mathcal{B}_n\}_{n \in \mathbb{N}}$ is said to converge to \mathcal{B} *uniformly*, denoted by $\mathcal{B}_n \rightarrow \mathcal{B}$, if $\lim_{n \rightarrow \infty} \|\mathcal{B}_n - \mathcal{B}\| = 0$. We also write $\mathcal{B} = \lim_{n \rightarrow \infty} \mathcal{B}_n$.
- 2) The sequence $\{\mathcal{B}_n\}_{n \in \mathbb{N}}$ is said to converge to \mathcal{B} *strongly*, denoted by $\mathcal{B}_n \rightarrow \mathcal{B}$, if $\lim_{n \rightarrow \infty} \|\mathcal{B}_n h - \mathcal{B}h\|_{\mathcal{F}} = 0$ for each $h \in \mathcal{F}$. We also write $\mathcal{B} = \text{s-lim}_{n \rightarrow \infty} \mathcal{B}_n$. \diamond

Remark 2.6: In analogy to the pointwise convergence of functions, the strong topology is the coarsest topology such that $\mathcal{B} \mapsto \mathcal{B}h$ is continuous in \mathcal{B} for each fixed $h \in \mathcal{F}$. \diamond

If \mathcal{A} is a bounded linear operator that generates $\{\mathcal{S}_t\}$, then $\mathcal{S}_t = e^{t\mathcal{A}}$ for each t in the uniform operator topology. Otherwise, [40, Chap. I, Theorem 5.5] (also rephrased as Theorem 2.8 in this paper) still provides an interpretation for the sense in which \mathcal{S}_t “equals” $e^{t\mathcal{A}}$.

We revisit some facts to show the above concepts of equivalence, particularly in the context where \mathcal{A} is unbounded.

Definition 2.7 (Resolvents): Let \mathcal{A} be a linear, not necessarily bounded, operator. Then the resolvent set is defined as

$$\rho(\mathcal{A}) := \{\lambda \in \mathbb{C} : \lambda \text{Id} - \mathcal{A} \text{ is invertible}\}. \quad (5)$$

For any $\lambda \in \rho(\mathcal{A})$, the resolvent operator is defined as

$$\mathcal{R}(\lambda; \mathcal{A}) := (\lambda \text{Id} - \mathcal{A})^{-1}, \quad (6)$$

and it is a bounded linear operator by [40, Chap. I, Theorem 4.3]. \diamond

We further define the *Yosida approximation* of \mathcal{A} as

$$\mathcal{A}_\lambda := \lambda \mathcal{A} \mathcal{R}(\lambda; \mathcal{A}) = \lambda^2 \mathcal{R}(\lambda; \mathcal{A}) - \lambda \text{Id}. \quad (7)$$

Note that $\{\mathcal{A}_\lambda\}_{\lambda \in \rho(\mathcal{A})}$ is a family of bounded linear operators, and $e^{t\mathcal{A}_\lambda}$ is well-defined for each $\lambda \in \rho(\mathcal{A})$.

Theorem 2.8: [40, Chap. I, Theorem 5.5] Suppose that $\{\mathcal{S}_t\}_{t \geq 0}$ is a \mathcal{C}_0 -semigroup on \mathcal{F} and \mathcal{A} is the generator. Then, $\mathcal{S}_t = \text{s-lim}_{\lambda \rightarrow \infty} e^{t\mathcal{A}_\lambda}$ for all $t \geq 0$.

III. THE CHARACTERIZATION OF THE INFINITESIMAL GENERATORS

For system (1), we are able to represent \mathcal{K}_t as $e^{t\mathcal{L}}$ for bounded \mathcal{L} , or, by Theorem 2.8, as the strong limit of $e^{t\mathcal{L}_\lambda}$, where \mathcal{L}_λ is the Yosida approximation of the unbounded \mathcal{L} .

For the converse representation of \mathcal{L} based on $\{\mathcal{K}_t\}_{t \geq 0}$, it is intuitive to take the operator logarithm such that $\mathcal{L} = \frac{1}{t} \log \mathcal{K}_t$. When \mathcal{L} is bounded, its spectrum’s sector should be confined to make the logarithm a single-valued mapping [36], [37]. However, for an unbounded \mathcal{L} , there is no direct connection \mathcal{L} and $\{\mathcal{K}_t\}_{t \geq 0}$.

In this subsection, we review how \mathcal{L} can be properly approximated based on $\{\mathcal{K}_t\}_{t \geq 0}$. For this purpose, we introduce the

following topologies. Let $\mathcal{C}(\Omega)$ be endowed with the uniform norm $|\cdot|_{\infty} := \sup_{x \in \Omega} |\cdot|$. Defining

$$|\cdot|_{\mathcal{L}} := |\cdot|_{\infty} + |\mathcal{L} \cdot|_{\infty}, \quad (8)$$

it can be shown that $|\cdot|_{\mathcal{L}}$ is equivalent to the \mathcal{C}^1 -uniform norm. Consequently $(\text{dom}(\mathcal{L}), |\cdot|_{\mathcal{L}})$ is a Banach space.

A. Asymptotic Approximations of Generators

First, we examine the base case where $\{\mathcal{K}_t\}_{t \geq 0}$ is a contraction semigroup. In this situation, by the famous Hille-Yosida theorem [40, Theorem 3.1, Chapter I], the resolvent set is such that $\rho(\mathcal{L}) \supseteq \mathbb{R}^+$, and for each $\lambda \in \rho(\mathcal{L})$, we have $\|\mathcal{R}(\lambda; \mathcal{L})\| \leq 1/\text{Re}(\lambda)$. Consequently, by [40, Lemma 1.3.3], $\{\mathcal{L}_\lambda\}_{\lambda > 0}$ converges in a strong sense to \mathcal{L} (w.r.t. $|\cdot|_{\mathcal{L}}$), i.e.,

$$\text{s-lim}_{\lambda \rightarrow \infty} \mathcal{L}_\lambda = \text{s-lim}_{\lambda \rightarrow \infty} \lambda^2 \mathcal{R}(\lambda; \mathcal{A}) - \lambda \text{Id} = \mathcal{L}. \quad (9)$$

Moreover, the convergence rate is $\lambda^{-1}|\mathcal{L}h|_{\mathcal{L}}$ for all $h \in \mathcal{C}^2(\Omega)$, i.e. $|\mathcal{L}_\lambda h - \mathcal{L}h|_{\infty} \leq \lambda^{-1}|\mathcal{L}h|_{\mathcal{L}}$.

Remark 3.1: Due to the contraction restriction of $\{\mathcal{K}_t\}_{t \geq 0}$, the system (1) is necessarily *dissipative* [40, Chapt. I, Theorem 4.3]. As characterized in [41], it is equivalent to verifying the existence of a value (storage) function $v : \Omega \rightarrow \mathbb{R}^+$ and a (supply) function $\eta : \Omega \rightarrow \mathbb{R}$ satisfying $\int_s^t |\mathcal{K}_\tau \eta(x)| d\tau < \infty$, for all $s \leq t$ and all $x \in \Omega$, such that $\mathcal{K}_{t-s} v(x) - v(x) \leq \int_s^t \mathcal{K}_\tau \eta(x) d\tau$. In other words, the energy storage rate of the system cannot exceed η . This assumption is somewhat restrictive when considering unknown systems. \diamond

To accommodate more general cases, we propose the following extension of the Yosida approximation on \mathbb{R}^+ . To achieve this, we first present the following facts.

Proposition 3.2: For system (1), there exist constants $\omega \geq 0$ and $C \geq 1$ such that $\|\mathcal{K}_t\| \leq C e^{\omega t}$ for all $t \geq 0$. In addition, for any $\lambda \in \mathbb{C}$, the family $\{\mathcal{K}_{t,\lambda}\}_{t \geq 0}$, where

$$\mathcal{K}_{t,\lambda} := e^{\lambda t} \mathcal{K}_t \quad (10)$$

is a \mathcal{C}_0 -semigroup with generator $\mathcal{L} + \lambda \text{Id} : \text{dom}(\mathcal{L}) \rightarrow \mathcal{C}(\Omega)$.

Proof: The first part follows directly by [40, Theorem 1.2.2]. The semigroup property of $\{\mathcal{K}_{t,\lambda}\}_{t \geq 0}$ follows easily by the definition. To verify its generator, we have

$$\frac{\mathcal{K}_{t,\lambda} h - h}{t} = \frac{e^{\lambda t} \mathcal{K}_t h - e^{\lambda t} h}{t} + \frac{e^{\lambda t} h - h}{t}. \quad (11)$$

For all $h \in \text{dom}(\mathcal{L})$, the limit exists as $t \downarrow 0$ for each r.h.s. term. It then follows that $\lim_{t \downarrow 0} \frac{\mathcal{K}_{t,\lambda} h - h}{t} = \mathcal{L} + \lambda \text{Id}$. \blacksquare

Although it has been demonstrated in extensive literature that $\text{s-lim}_{\lambda \rightarrow \infty} \mathcal{L}_\lambda = \mathcal{L}$ for $\{\mathcal{L}_\lambda\}_{\lambda > \omega}$, to better understand how data-driven approaches can be integrated into the approximation scheme, we prove the following theorem and demonstrate an explicit convergence rate.

Theorem 3.3: For system (1), consider $\{\mathcal{L}_\lambda\}_{\lambda > \tilde{\omega}}$, where $\tilde{\omega} \geq \omega > 0$. Then, $\text{s-lim}_{\lambda \rightarrow \infty} \mathcal{L}_\lambda = \mathcal{L}$. Moreover, for any $h \in \mathcal{C}^2(\Omega)$, there exists an $\tilde{C} > 0$ such that

$$|\mathcal{L}_\lambda h - \mathcal{L}h|_{\infty} \leq \tilde{C}(\lambda - \tilde{\omega})^{-1}(|h|_{\mathcal{L}} + |\mathcal{L}h|_{\mathcal{L}}).$$

Proof: For any $\tilde{\omega} \geq \omega$, we consider $\{\mathcal{K}_{t,-\tilde{\omega}}\}_{t \geq 0}$, where $\mathcal{K}_{t,-\tilde{\omega}}$ is defined as (10). It is clear that $\|\mathcal{K}_{t,-\tilde{\omega}}\| \leq C$ for all $t \geq$

0. By Proposition 3.2, $\{\mathcal{K}_{t,-\tilde{\omega}}\}_{t \geq 0}$ also admits the generator $\mathcal{L} - \tilde{\omega} \text{Id}$. Within $\mathcal{C}^1(\Omega)$, for any $\lambda > \tilde{\omega}$, we have

$$\begin{aligned} \mathcal{L} - \mathcal{L}_\lambda &= \mathcal{L} - \tilde{\omega} \text{Id} + \tilde{\omega} \text{Id} - \mathcal{L}_\lambda \\ &= (\mathcal{L} - \tilde{\omega} \text{Id} - (\mathcal{L} - \tilde{\omega} \text{Id})_{\lambda - \tilde{\omega}}) \\ &\quad + ((\mathcal{L} - \tilde{\omega} \text{Id})_{\lambda - \tilde{\omega}} + \tilde{\omega} \text{Id} - \mathcal{L}_\lambda) \\ &=: \mathcal{O}_1 + \mathcal{O}_2, \end{aligned} \quad (12)$$

where $(\mathcal{L} - \tilde{\omega} \text{Id})_{\lambda - \tilde{\omega}}$ is the Yosida approximation of $\mathcal{L} - \tilde{\omega} \text{Id}$. It suffices to show the bound for each of the two terms on the r.h.s. of (12).

To show the bound for \mathcal{O}_1 , we consider an alternative norm for $h \in \mathcal{C}^1(\Omega)$, defined as $\|h\|_\infty = \sup_{t \geq 0} |\mathcal{K}_{t,-\tilde{\omega}} h|_\infty$. It can be verified that $|h|_\infty \leq \|h\|_\infty \leq C|h|_\infty$. For $|h|_\mathcal{L}$, we define the alternative norm $\|h\|_\mathcal{L} = \|h\|_\infty + \|\mathcal{L}h\|_\infty$. In addition, $\|\mathcal{K}_{t,-\tilde{\omega}} h\|_\infty = \sup_{s \geq 0} |\mathcal{K}_{s,-\tilde{\omega}} \mathcal{K}_{t,-\tilde{\omega}} h|_\infty \leq \sup_{s \geq 0} |\mathcal{K}_{s,-\tilde{\omega}} h|_\infty = \|h\|_\infty$, which demonstrates the contraction property w.r.t. $\|\cdot\|_\infty$. Then, by the definition of the resolvent operator, we have $((\lambda - \tilde{\omega})I - (\mathcal{L} - \tilde{\omega} \text{Id}))\mathcal{R}(\lambda - \tilde{\omega}; \mathcal{L} - \tilde{\omega} \text{Id}) = \text{Id}$, which implies

$$((\lambda - \tilde{\omega})I - (\mathcal{L} - \tilde{\omega} \text{Id}))\mathcal{R}(\lambda - \tilde{\omega}; \mathcal{L} - \tilde{\omega} \text{Id})(\mathcal{L} - \tilde{\omega} \text{Id}) = \mathcal{L} - \tilde{\omega} \text{Id}. \quad (13)$$

Recall the definition of the Yosida approximation for $(\mathcal{L} - \tilde{\omega} \text{Id})_{\lambda - \tilde{\omega}}$. For any $h \in \mathcal{C}^2(\Omega)$, by expanding (13), we can obtain $\mathcal{O}_1 h = -(\mathcal{L} - \tilde{\omega} \text{Id})\mathcal{R}(\lambda - \tilde{\omega}; \mathcal{L} - \tilde{\omega} \text{Id})(\mathcal{L} - \tilde{\omega} \text{Id})h$. Consequently,

$$\begin{aligned} |\mathcal{O}_1 h|_\infty &\leq \|\mathcal{O}_1 h\|_\infty \leq (\lambda - \tilde{\omega})^{-1} \|(\mathcal{L} - \tilde{\omega} \text{Id})h\|_{\mathcal{L} - \tilde{\omega} \text{Id}} \\ &\leq C(\lambda - \tilde{\omega})^{-1} \|(\mathcal{L} - \tilde{\omega} \text{Id})h\|_{\mathcal{L} - \tilde{\omega} \text{Id}} \\ &\leq C(\lambda - \tilde{\omega})^{-1} (|\mathcal{L}h|_\mathcal{L} + \tilde{\omega}|h|_\mathcal{L} + \tilde{\omega}|h|_\infty) \\ &\leq C(\lambda - \tilde{\omega})^{-1} (|\mathcal{L}h|_\mathcal{L} + (2\tilde{\omega} + 1)|h|_\mathcal{L}), \end{aligned}$$

where the second inequality can be proved in the same way as in [40, Chap. I, Lemma 3.2], and the last two inequalities are based on the definitions of the norms $|\cdot|_{\mathcal{L} - \tilde{\omega} \text{Id}}$ and $|\cdot|_\mathcal{L}$, obtained by expanding them. Since $\mathcal{C}^2(\Omega)$ is dense in $\mathcal{C}^1(\Omega)$, and the operator \mathcal{O}_1 is uniformly bounded [40, Theorem 1.3.1] and hence continuous on $\mathcal{C}^1(\Omega)$, we have

$$\mathcal{L} - \tilde{\omega} \text{Id} = \text{s-lim}_{\lambda \rightarrow \infty} (\mathcal{L} - \tilde{\omega} \text{Id})_{\lambda - \tilde{\omega}} \quad (14)$$

on $(\mathcal{C}^1(\Omega), \|\cdot\|_\mathcal{L})$. Due to the norm equivalence between $\|\cdot\|_\mathcal{L}$ and $|\cdot|_\mathcal{L}$, the convergence (14) also holds on $(\mathcal{C}^1(\Omega), |\cdot|_\mathcal{L})$.

We now work on the bound for \mathcal{O}_2 . One can show by a direct calculation that, for any $h \in \mathcal{C}^1(\Omega)$,

$$\begin{aligned} |\mathcal{O}_2 h|_\infty &= |2\tilde{\omega}h - \tilde{\omega}(2\lambda - \tilde{\omega})R(\lambda; \mathcal{L})h|_\infty \\ &= |\tilde{\omega}(\tilde{\omega}R(\lambda; \mathcal{L}) - 2\mathcal{L}R(\lambda; \mathcal{L}))h|_\infty \\ &\leq C(\lambda - \tilde{\omega})^{-1} (\tilde{\omega}^2|h|_\infty + 2\tilde{\omega}|\mathcal{L}h|_\infty) \\ &\leq C_0(\lambda - \tilde{\omega})^{-1} |h|_\mathcal{L}, \end{aligned} \quad (15)$$

where $C_0 = C \cdot \max\{\tilde{\omega}^2, 2\tilde{\omega}\}$.

The conclusion follows by combining both parts and considering $\lambda \rightarrow \infty$. ■

Remark 3.4: In the proof of Theorem 3.3, we have implicitly demonstrated the effects of C and ω in the semigroup estimation $\|\mathcal{K}_t\| \leq C e^{\omega t}$. Intuitively, C represents the uniform

scaling of the magnitude of the Koopman operator, while ω indicates the dominant exponential growth or decay rate of the flow on $\mathcal{C}(\Omega)$.

Specifically, one can shift the original generator \mathcal{L} to a stable generator $\mathcal{L} - \tilde{\omega} \text{Id}$, which generates a contraction semigroup w.r.t. a norm equivalent to $|\cdot|_\infty$, and then shift back to \mathcal{L} by adding $\tilde{\omega} \text{Id}$. The analysis in the proof determines the error (\mathcal{O}_1) between the stable generator $\mathcal{L} - \tilde{\omega} \text{Id}$ and its Yosida approximation, as well as the error (\mathcal{O}_2) between the approximation \mathcal{L}_λ of the original generator and the approximation $(\mathcal{L} - \tilde{\omega} \text{Id})_{\lambda - \tilde{\omega}} + \tilde{\omega} \text{Id}$ of the ‘‘shift-back’’ operator.

Note that this shifting strategy used in the proof is advantageous for applying the analysis of contraction semigroups, but the shift inevitably increases the cost. Nonetheless, the overall error of using the Yosida approximation on $\rho(\mathcal{L})$ is always dominated by a reciprocal term. ◊

B. Representation of Resolvent Operators

Motivated by representing \mathcal{L} by $\{\mathcal{K}_t\}_{t \geq 0}$ and the Yosida approximation for \mathcal{L} on $\{\lambda > \omega\}$, we establish a connection between $\mathcal{R}(\lambda; \mathcal{L})$ and $\{\mathcal{K}_t\}_{t \geq 0}$.

Proposition 3.5: Let $\mathcal{R}(\lambda)$ on $\mathcal{C}(\Omega)$ be defined by

$$\mathcal{R}(\lambda)h := \int_0^\infty e^{-\lambda t} (\mathcal{K}_t h) dt. \quad (16)$$

Then, for all $\lambda > \omega$,

- 1) $\mathcal{R}(\lambda)(\lambda \text{Id} - \mathcal{L})h = h$ for all $h \in \mathcal{C}^1(\Omega)$;
- 2) $(\lambda \text{Id} - \mathcal{L})\mathcal{R}(\lambda)h = h$ for all $h \in \mathcal{C}(\Omega)$.

The proof follows the standard procedures of calculus and dynamic programming, and is completed in Appendix A.

Remark 3.6: Even though $\mathcal{R}(\lambda)$ is well defined on $\mathcal{C}(\Omega)$, the commutative property between $\mathcal{R}(\lambda)$ and $\lambda \text{Id} - \mathcal{L}$ only holds on $\mathcal{C}^1(\Omega)$. Consequently, $R(\lambda; \mathcal{L})$ and $R(\lambda)$ are equivalent only on $\mathcal{C}^1(\Omega)$. This domain aligns with the valid domain where $\mathcal{L} = \text{s-lim}_{\lambda \rightarrow \infty} \mathcal{L}_\lambda$. ◊

To use the approximation in Section III-A, we can replace $R(\lambda; \mathcal{L})$ with $R(\lambda)$. We can immediately conclude the following representation.

Corollary 3.7: For each $\lambda > \omega$,

$$\mathcal{L}_\lambda = \lambda^2 \int_0^\infty e^{-\lambda t} \mathcal{K}_t dt - \lambda \text{Id} \quad (17)$$

and $\mathcal{L}_\lambda \rightarrow \mathcal{L}$ on $\mathcal{C}^1(\Omega)$.

IV. KOOPMAN-BASED FINITE-DIMENSIONAL APPROXIMATION OF GENERATORS

The current form of $\int_0^\infty e^{-\lambda t} (\mathcal{K}_t \cdot) dt$ in (17) is not advantageous for data-driven approximation. In this section, we derive a finite-horizon, finite-dimensional approximation, demonstrating the feasibility of using observable data to learn the generator.

A. Finite Time-Horizon Approximation

Observing the form of (17), we first define the following truncation integral operator.

Definition 4.1: For any $h \in \mathcal{C}(\Omega)$ and $\tau_s \geq 0$, we define $\mathcal{R}_{\lambda, \tau_s} : \mathcal{C}(\Omega) \rightarrow \mathcal{C}(\Omega)$ as

$$\mathcal{R}_{\lambda, \tau_s} h(x) := \int_0^{\tau_s} e^{-\lambda s} \mathcal{K}_s h(x) ds. \quad (18)$$

We aim to demonstrate that for any sufficiently large $\lambda \in \mathbb{R}$, the aforementioned truncation of the integral will not significantly “hurt” the accuracy of the approximation (17).

Theorem 4.2: Let $\tau_s \geq 0$ and $\lambda > \omega$ be fixed. Then, $\|\lambda^2 \mathcal{R}_{\lambda, \tau_s} - \lambda \text{Id} - \mathcal{L}_\lambda\| \leq \frac{C\lambda^2}{\lambda - \omega} e^{-\lambda \tau_s}$ on $\mathcal{C}^1(\Omega)$.

Proof: Note that, for any $\lambda > \omega$,

$$\begin{aligned} \|\mathcal{R}(\lambda)\| &\leq \int_0^\infty e^{-\lambda t} \|\mathcal{K}_t\| dt \\ &\leq \int_0^\infty C e^{-\lambda t} e^{\omega t} dt = \frac{C}{\lambda - \omega}. \end{aligned} \quad (19)$$

Therefore, for any $h \in \mathcal{C}(\Omega)$,

$$\begin{aligned} |\mathcal{R}_{\lambda, \tau_s} h - \mathcal{R}(\lambda; \mathcal{L})h|_\infty &= \sup_{x \in \Omega} |e^{-\lambda \tau_s} \mathcal{R}(\lambda)h(\phi(\tau_s, x))| \\ &\leq e^{-\lambda \tau_s} \|\mathcal{R}(\lambda)\| \|h\|_\infty \leq e^{-\lambda \tau_s} \frac{C}{\lambda - \omega} \|h\|_\infty \end{aligned} \quad (20)$$

and $\sup_{|h|_\infty=1} |\lambda^2 \mathcal{R}_{\lambda, \tau_s} h - \lambda h - \mathcal{L}_\lambda h|_\infty \leq \frac{C\lambda^2}{\lambda - \omega} e^{-\lambda \tau_s}$, which completes the proof. ■

We notice that, for any fixed τ_s , the error bound $\frac{C\lambda^2}{\lambda - \omega} e^{-\lambda \tau_s}$ in Theorem 4.2 demonstrates an exponential decaying rate in the uniform sense as $\lambda \rightarrow \infty$. Recalling the convergence rate of $\mathcal{L}_\lambda \rightarrow \mathcal{L}$ in Theorem 3.3, we note that the convergence in Theorem 4.2 does not dominate for any fixed $\tau_s > 0$. This allows us to use

$$\mathcal{L}_{\lambda, \tau_s} := \lambda^2 \mathcal{R}_{\lambda, \tau_s} - \lambda \text{Id} \quad (21)$$

to approximate \mathcal{L} within a small time horizon. We use the following example to illustrate this approximation.

Example 4.3: Consider the simple dynamical system $\dot{x} = x$ and the observable function $v(x) = x^n$ for any $n \geq 1$. Then, analytically, $\phi(s, x) = xe^s$ for all $s \geq 0$ and $\mathcal{L}v(x) = nx^n$. We test the validity of using Eq. (21). Note that, for sufficiently large λ , we have $\lambda^2 \int_0^{\tau_s} e^{-\lambda s} (\mathcal{K}_s v(x)) ds = \lambda^2 \int_0^{\tau_s} e^{-\lambda s} e^{sn} x^n ds = \lambda^2 x^n \int_0^{\tau_s} e^{-(\lambda - n)s} ds = \frac{\lambda^2 x^n}{\lambda - n} (1 - e^{-(\lambda - n)\tau_s}) \approx \frac{\lambda^2 x^n}{\lambda - n}$, and $\lambda^2 \mathcal{R}_{\lambda, \tau_s} v(x) - \lambda v(x) \approx \frac{\lambda^2 x^n}{\lambda - n} - \lambda x^n = \frac{n\lambda}{\lambda - n} x^n \approx nx^n = \mathcal{L}v(x)$. With high-accuracy evaluation of the truncated integral, we can achieve a reasonably good approximation. ◊

B. Finite-Rank Approximation

Based on (21), it suffices to learn the operator $\mathcal{R}_{\lambda, \tau_s}$ for any fixed $\tau_s > 0$ and to predict the image of the operator when acting on some $\mathcal{C}(\Omega)$ function. In favor of a machine learning approach based on a dictionary of a finite number of observable test functions serving as basis functions, we verify if $\mathcal{R}_{\lambda, \tau_s}$ is representable as a finite-rank operator.

We first look at the following property of $\mathcal{R}_{\lambda, \tau_s}$.

Proposition 4.4: For any $\lambda > \omega$, the operator $\mathcal{R}_{\lambda, \tau_s}$ is compact if and only if \mathcal{K}_s is compact for any $s \in (0, \tau_s]$.

Proof: We assume that $\mathcal{R}_{\lambda, \tau_s}$ is compact for $\lambda > \omega$. By [40, Theorem 3.2], \mathcal{K}_s is continuous w.r.t. the uniform operator norm $\|\cdot\|$. We can also easily verify the compactness of $\lambda \mathcal{R}_{\lambda, \tau_s} \mathcal{K}_s$, for any $s \in (0, \tau_s]$, by Definition 4.1. In addition, for any arbitrarily small $t > 0$,

$$\begin{aligned} &\|\lambda \mathcal{R}_{\lambda, \tau_s} \mathcal{K}_s - \mathcal{K}_s\| \\ &\leq \int_0^t \lambda e^{-\lambda \sigma} \|\mathcal{K}_{s+\sigma} - \mathcal{K}_s\| d\sigma + \int_t^{\tau_s} \lambda e^{-\lambda \sigma} \|\mathcal{K}_{s+\sigma} - \mathcal{K}_s\| d\sigma \\ &\leq \sup_{\sigma \in (0, t]} \|\mathcal{K}_{s+\sigma} - \mathcal{K}_s\| (1 - e^{-\lambda t}) + 2 \int_t^{\tau_s} \lambda e^{-\lambda \sigma} \|\mathcal{K}_{\tau_s}\| d\sigma \\ &\leq \sup_{\sigma \in (0, t]} \|\mathcal{K}_{s+\sigma} - \mathcal{K}_s\| + \frac{2C\lambda}{\lambda - \omega} e^{\omega(t + \tau_s) - \lambda t}. \end{aligned}$$

By the continuity of \mathcal{K}_s , letting $\lambda \rightarrow \infty$ and $t \rightarrow 0$, we have $\mathcal{K}_s \rightarrow \lambda \mathcal{R}_{\lambda, \tau_s} \mathcal{K}_s$ in the uniform sense, which shows the compactness.

To show the converse side, we notice that the operator $\mathcal{R}_{\lambda, \tau_s}^t := \int_t^{\tau_s} e^{-\lambda s} \mathcal{K}_s ds$ is always compact for any $t \in (0, \tau_s]$ given the compactness of \mathcal{K}_s with $s \in (0, \tau_s]$. However,

$$\begin{aligned} \|\mathcal{R}_{\lambda, \tau_s} - \mathcal{R}_{\lambda, \tau_s}^t\| &\leq \int_0^t e^{-\lambda s} \|\mathcal{K}_s\| ds \leq \int_0^t \|\mathcal{K}_s\| ds \\ &\leq \int_0^t C e^{\omega s} ds \leq t C e^{\omega t}. \end{aligned}$$

Letting $t \rightarrow 0$, we see the uniform convergence of $\mathcal{R}_{\lambda, \tau_s}^t$ to $\mathcal{R}_{\lambda, \tau_s}$, which shows compactness of $\mathcal{R}_{\lambda, \tau_s}$. ■

It is worth noting that \mathcal{K}_t of (1) is not necessarily compact for each $t > 0$. To show that $\mathcal{K}_t(B_r) \subseteq \mathcal{C}(\Omega)$ is relatively compact, where $B_r = \{h \in \mathcal{C}(\Omega) : |h|_\infty \leq r\}$ for some $r > 0$, one needs to verify the equicontinuity within $\mathcal{K}_t(B_r)$. However, this is not guaranteed. As a counterexample, we set $\Omega := (-1, 1)$, $h_n(x) = \sin(nx) \in B_1$ (or similarly, for the Fourier basis), and define $\phi(t, x) = e^{-t}x$ for all $x \in \Omega$. Then, the sequence $h_n \circ \phi(t, \cdot)$ for each t does not exhibit equicontinuity due to the rapid oscillation as n increases.

For the purpose of approximating \mathcal{L} strongly, we aim to find a compact approximation of $\{\mathcal{K}_t\}_{t>0}$ that enables a finite-rank representation of $\mathcal{R}_{\lambda, \tau_s}$ in the same sense.

Proposition 4.5: For each $t > 0$, there exists a family of compact linear operator $\{\mathcal{K}_t^\varepsilon\}_{\varepsilon>0}$, such that $\mathcal{K}_t^\varepsilon \rightarrow \mathcal{K}_t$ on $\mathcal{C}(\Omega)$ as $\varepsilon \rightarrow 0$. In addition, for each $t, s > 0$, there exists a family of compact linear operator $\{\mathcal{K}_t^\varepsilon\}_{\varepsilon>0}$, such that $\mathcal{K}_t^\varepsilon \circ \mathcal{K}_s^\varepsilon \rightarrow \mathcal{K}_t \circ \mathcal{K}_s$ on $h \in \mathcal{C}(\Omega)$ as $\varepsilon \rightarrow 0$.

We omit the proof, as it follows similar arguments presented in [27, Section V.A]. Heuristically, the semigroup $\{\mathcal{K}_t\}_{t>0}$ characterizes the flow of point masses of the system (1), where each point mass is considered to be distributed by a Dirac measure centered at its respective point in the flow. The compact approximation is achieved through the introduction of smooth mollifiers. Taking advantage of the compactness approximation, the following statement demonstrates the feasibility of approximating $\mathcal{R}_{\lambda, \tau_s}$ by a finite-dimensional operator.

Corollary 4.6: For any fixed $\tau > 0$, for any arbitrarily small $\delta > 0$, there exists a sufficiently large N and a

finite-dimensional approximation $\mathcal{R}_{\lambda, \tau_s}^N$ such that $|\mathcal{R}_{\lambda, \tau_s}^N h - \mathcal{R}_{\lambda, \tau_s} h|_\infty < \delta$, $h \in \mathcal{C}(\Omega)$.

The proof is completed in Appendix A.

Remark 4.7: Similar to [27, Section V.B], one can consider a Hilbert space $\mathcal{H} := L^2(\Omega) \supseteq \mathcal{C}(\Omega)$ as a special case. Let $\{\varphi_i\}_{i \in \mathbb{Z}} \subseteq \mathcal{H}$ be the possibly complex-valued eigenfunctions of $\mathcal{K}_t^\varepsilon$. Then, $\mathcal{K}_t^\varepsilon \cdot = \sum_{i \in \mathbb{Z}} \rho_i^\varepsilon \langle \cdot, \bar{\varphi}_i \rangle \varphi_i$ can be approximated by a finite-sum $\mathcal{K}_t^N \cdot = \sum_{i=-N}^N \rho_i^\varepsilon \langle \cdot, \bar{\varphi}_i \rangle \varphi_i$, where $\{\rho_i^\varepsilon\}_{i \in \mathbb{Z}}$ represents the set of eigenvalues of $\{\mathcal{K}_t^\varepsilon\}_{t \geq 0}$ and $\langle \bar{\varphi}_i, \varphi_i \rangle = 1$ for all i . Then, $\mathcal{R}_{\lambda, \tau_s}^N$ can be defined accordingly as shown in the proof of Corollary 4.6. \diamond

When dealing with linear operators in finite-dimensional spaces, the concept of basis equivalence ensures that different representations corresponding to different bases are related through similarity transformations. Thus, the operator's inherent properties remain invariant under a change of basis. Building on the feasibility of finite-dimensional approximation, the next section will investigate how to train $\mathcal{L}_{\lambda, \tau_s}$ using a finite dictionary of test functions.

V. DATA-DRIVEN ALGORITHM

We continue to discuss the data-driven learning based on the approximations discussed in Section IV (recall Definition 4.1, Eq. (21), and Corollary 4.6). Similar to the learning of Koopman operators [27], [33], [42], obtaining a fully discretized version L of the bounded linear operator $\lambda^2 \mathcal{R}_{\lambda, \tau_s}^N - \lambda \text{Id}$ based on the training data typically relies on the selection of a discrete dictionary of continuously differentiable observable test functions, denoted by

$$\mathcal{Z}_N(x) := [\mathfrak{z}_0(x), \mathfrak{z}_1(x), \dots, \mathfrak{z}_{N-1}(x)], \quad N \in \mathbb{N}. \quad (22)$$

Then, the following are expected to hold: 1) Let $(\mu_i, \xi_i)_{i=0}^{N-1}$ be the eigenvalues and eigenvectors of L . Let $(\rho_i, \varphi_i)_{i=0}^{N-1}$ be the eigenvalues and eigenfunctions of \mathcal{L} . Then, for each i ,

$$\mu_i \approx \rho_i, \quad \varphi_i(x) \approx \mathcal{Z}_N(x) \xi_i. \quad (23)$$

2) For any $h \in \text{span}\{\mathfrak{z}_0, \mathfrak{z}_1, \dots, \mathfrak{z}_{N-1}\}$ such that $h(x) = \mathcal{Z}_N(x) \theta$ for some column vector θ , we have that

$$\mathcal{L}h(\cdot) \approx \mathcal{L}_{\lambda, \tau_s} h(\cdot) \approx \lambda^2 \mathcal{R}_{\lambda, \tau_s}^N h(\cdot) - \lambda h(\cdot) \approx \mathcal{Z}_N(\cdot)(L\theta). \quad (24)$$

We can let $\tilde{\mathcal{L}}h(x) := \mathcal{Z}_N(x)(L\theta)$ for simplicity. In this section, we modify the existing Koopman learning technique to obtain L such that (23) and (24) hold.

Remark 5.1: The approximation in (24) can also guarantee the convergence of $e^{t\mathcal{Z}_N(x)(L\theta)}$ to the original semigroup $\{\mathcal{K}_t\}_{t \geq 0}$ for any $h(x) = \mathcal{Z}_N(x)\theta$. Indeed, letting $\mathcal{O} = \tilde{\mathcal{L}} - \mathcal{L}_\lambda$, we have

$$\begin{aligned} & |e^{t\tilde{\mathcal{L}}}h - \mathcal{K}_t h|_\infty \\ & \leq \|e^{t\mathcal{O}}\| \|e^{t\mathcal{L}_\lambda}h - \mathcal{K}_t h\|_\infty + \|\mathcal{K}_t\| \|e^{t\mathcal{O}}h - h\|_\infty \\ & \leq \|e^{t\mathcal{O}}\| \|e^{t\mathcal{L}_\lambda}h - \mathcal{K}_t h\|_\infty + t\|\mathcal{K}_t\| \|e^{t\mathcal{O}}\| \|\mathcal{O}h\|_\infty. \end{aligned} \quad (25)$$

Note that \mathcal{O} and \mathcal{K}_t (for any t) are bounded operators. As $N, \lambda \rightarrow \infty$, the first part goes to 0 by Theorem 2.8. The second part goes to 0 by the sequence of approximations (in a strong sense) in (24). \diamond

A. Generating Training Data

The training data is obtained in the following way. By randomly sampling M initial conditions $\{x^{(m)}\}_{m=0}^{M-1} \subseteq \Omega$ and fixing a τ_s , we stack the *features* into X , such that:

$$X = [\mathcal{Z}_N(x^{(0)}), \mathcal{Z}_N(x^{(1)}), \dots, \mathcal{Z}_N(x^{(M-1)})]^\top. \quad (26)$$

For any fixed $\lambda > 0$, given a dictionary \mathcal{Z}_N of the form (22), for each $\mathfrak{z}_i \in \mathcal{Z}_N$ and each $x^{(m)}$, we consider $\lambda^2 \mathcal{R}_{\lambda, \tau_s} \mathfrak{z}_i(x^{(m)}) - \lambda \mathfrak{z}_i(x^{(m)}) = \lambda^2 \int_0^{\tau_s} e^{-\lambda s} \mathfrak{z}_i(\phi(s, x^{(m)})) ds - \lambda \mathfrak{z}_i(x^{(m)})$ as the labels. To compute the integral, we employ numerical quadrature techniques for approximation. This approach inevitably requires discrete-time observations (snapshots) with an observation/sampling rate of γ Hz within the interval $[0, \tau_s]$ of each flow map $\phi(\tau_s, x^{(m)})$. We denote the number of snapshots as $\Gamma := \gamma \tau_s$. We stack the snapshot data in the following intermediate matrix:

$$\begin{aligned} U^{(m)} & (= U_\Gamma^{(m)}) \\ & = \lambda^2 [\mathcal{Z}_N(\phi(0, x^{(m)})), \dots, e^{-\frac{\lambda k \tau_s}{\Gamma}} \mathcal{Z}_N(\phi(\frac{k \tau_s}{\Gamma}, x^{(m)})), \\ & \quad \dots e^{-\frac{\lambda \tau_s}{\Gamma}} \mathcal{Z}_N(\phi(\tau, x^{(m)}))]^\top, \quad m \in \{0, 1, \dots, M-1\}. \end{aligned} \quad (27)$$

Denote by $\mathcal{G}_{[0, \tau_s]}^\lambda(v)$, or simply $\mathcal{G}(v)$ for brevity, the Gauss–Legendre quadrature² based on the vector of points v within $[0, \tau_s]$, and denote by $U^{(m)}[:, j]$ the j^{th} column of $U^{(m)}$. The stack of labels is given by³

$$Y (= Y_{\lambda, \tau_s}^\Gamma) := \mathcal{I}_{\lambda, \tau_s}^\Gamma - \lambda X, \quad (28)$$

where

$$\mathcal{I}_{\lambda, \tau_s}^\Gamma = \begin{bmatrix} \mathcal{G}(U^{(0)}[:, 0]) & \dots & \mathcal{G}(U^{(0)}[:, N-1]) \\ \vdots & \ddots & \vdots \\ \mathcal{G}(U^{(m)}[:, 0]) & \dots & \mathcal{G}(U^{(m)}[:, N-1]) \\ \vdots & \ddots & \vdots \\ \mathcal{G}(U^{(M-1)}[:, 0]) & \dots & \mathcal{G}(U^{(M-1)}[:, N-1]) \end{bmatrix}. \quad (29)$$

We omit the algorithm for generating the training data (X, Y) , as it follows straightforwardly from the data stacking shown in (26) and (28).

B. Extended Dynamic Mode Decomposition Algorithm

After obtaining (X, Y) , we can find L by $L = \text{argmin}_{A \in \mathbb{C}^{N \times N}} \|Y - XA\|_F$. The L is given in closed-form as $L = (X^\top X)^\dagger X^\top Y$. Similar to Extended Dynamic Mode Decomposition (EDMD) [42] for learning Koopman operators, the approximations (23) and (24) can be guaranteed.

²Given the Laplace transform-type integral, we choose to use the Gauss–Legendre quadrature rule to improve accuracy for relatively smaller values of Γ . We omit the details of implementing the Gauss–Legendre quadrature numerically, as the algorithms are well-established in this field.

³The superscripts and subscripts in the notation indicate the dependence of the parameters, reflecting that the image function values of the generator are only achieved approximately. The λ and τ_s determine the analytical error, while the Γ determines the numerical error. When the dependence on any parameter is not emphasized, we can use shorthand notation without the corresponding superscript and subscript.

C. Modification Under Low Sampling Rate Constraints

Recall that $Y (= Y_{\lambda, \tau_s}^\Gamma)$, or equivalently, $\mathcal{I}_{\lambda, \tau_s}^\Gamma$, is obtained through both analytical and numerical approximations. Among the three parameters, λ , τ_s , and Γ , τ_s is less important than the others according to Theorem 4.2, so we can set τ_s to be a relatively small fixed value. On the other hand, λ and Γ need to be large to reduce the error.

Empirically, for larger λ under any fixed $\tau_s > 0$, the numerical integration requires a larger Γ , which corresponds to a higher sampling frequency. Conversely, if Γ is restrictive in practice (for example, in automatic vehicles or intelligent transportation systems, where sensors can collect state data at no more than a 100 Hz sensing rate), λ cannot be large to ensure accuracy when using numerical integration. Making λ and Γ both sufficiently large cannot be achieved without modifications based on (28).

To resolve this conflict, we employ the first resolvent identity

$$[(\lambda - \mu)\mathcal{R}(\mu) + \text{Id}]\mathcal{R}(\lambda) = \mathcal{R}(\mu) \quad (30)$$

to connect two resolvent operators with different values λ and μ in the resolvent set. This identity allows us to learn a resolvent operator with a small μ (thus enabling the use of a small Γ for numerical integration) and then infer the resolvent operator with a large λ . To adapt this inference step into generator learning based on (28), we provide the formula for the modified L as

$$L_{\text{mod}} = A^\dagger B, \quad (31)$$

where

$$A = \frac{\lambda - \mu}{\mu^2} \mathcal{I}_\mu + X, \text{ and } B = \frac{\lambda}{\mu} \mathcal{I}_\mu - \lambda X, \quad (32)$$

and $\mathcal{I}_\mu (= \mathcal{I}_{\mu, \tau_s}^\Gamma)$ is evaluated for a small μ . We provide the derivation in Appendix B.

D. Discussion of Other Existing Methods

Recall Remark 2.4 on the FDM with an expression $\frac{\mathcal{K}_\tau - \text{Id}}{\tau} \triangleq \mathcal{L}$, where the convergence is well studied in [28]. We also revisit the benchmark Koopman Logarithm Method (KLM) based on the expression $\mathcal{L} = \frac{1}{\tau} \log(\mathcal{K}_\tau)$, as described in [33]. In this subsection, we discuss the data-driven algorithms for FDM and KLM, in preparation for the comparison in the case studies in Section VI.

Observing that the expressions for \mathcal{L} in FDM and KLM rely on just one moment of the Koopman operator \mathcal{K}_τ , the data-driven versions of these methods are divided into two steps: 1) learning \mathcal{K}_τ ; 2) transforming the learned \mathcal{K}_τ to \mathcal{L} , respectively. To make the sampling rate consistent with the RTM, we set $\tau := \tau_s/\Gamma$.

The corresponding data-driven approximations also rely on the selection of a discrete dictionary \mathcal{Z}_N , and similarly, the approximation is to achieve $\mathcal{L}h(\cdot) \approx \mathcal{Z}_N(\cdot)(L_i\theta)$ for $h(x) = \mathcal{Z}_N(x)\theta$ and for any $i \in \{\text{FDM, KLM}\}$. To do this, we fix a τ , and stack the *features* into X the same way as (26). The *labels* are stacked into Z :

$$Z = [\mathcal{Z}_N(\phi(\tau, x^{(0)}), \dots, \mathcal{Z}_N(\phi(\tau, x^{(M-1)}))]^\top. \quad (33)$$

After obtaining the training data (X, Z) , we can find K (the fully discretized version of \mathcal{K}_τ) by $K = \arg\min_{A \in \mathbb{C}^{N \times N}} \|Z - XA\|_F$. The K is given in closed-form as $K = (X^\top X)^\dagger X^\top Z$ [42]. The data-driven approximation for \mathcal{L} based on FDM and KLM can be immediately obtained using K .

1) FDM: $L_{\text{FDM}} = (K - \text{Id})/\tau$, where $\text{Id} = \text{Id}_{N \times N}$ is the identity matrix in this expression.

2) KLM: $L_{\text{KLM}} = \log(K)/\tau$.

Remark 5.2: Let $(\mu_i^K, \xi_i^K)_{i=0}^{N-1}$ be the eigenvalues and eigenvectors of K . Let $(\rho_i^K, \varphi_i^K)_{i=0}^{N-1}$ be the eigenvalues and eigenfunctions of \mathcal{K}_τ . Similar to (23) and (24), for each i , we have $\varphi_i^K(x) \approx \mathcal{Z}_N(x)\xi_i^K$ and $\mathcal{K}_s h(\cdot) \approx \mathcal{Z}_N(\cdot)(K\theta)$ for $h(x) = \mathcal{Z}_N(x)\theta$. \diamond

It is worth noting that, even when \mathcal{L} can be represented by $(\log \mathcal{K}_\tau)/\tau$, we cannot guarantee that $\frac{\log \mathcal{K}_\tau}{\tau} h(\cdot) \approx \mathcal{Z}_N(\cdot)(\frac{\log(K)}{\tau}\theta)$ as in KLM, not to mention the case where the above logarithm representation does not hold. Denoting $\Phi(\cdot) = [\varphi_0^K(\cdot), \varphi_1^K(\cdot), \dots, \varphi_{N-1}^K(\cdot)]$ and $\Xi = [\xi_0^K, \xi_1^K, \dots, \xi_{N-1}^K]$, then it is clear that $\Phi(\cdot) = \mathcal{Z}_N(\cdot)\Xi$. In view of Remark 4.7, any $\mathcal{K}_\tau h(x)$ for any $h(x) = \mathcal{Z}_N(x)\theta$ can be approximated using Φ . The (possibly complex-valued) rotation matrix Ξ establishes the connection between finite-dimensional eigenfunctions and dictionary functions through data-fitting, ensuring that any linear combination within \mathcal{Z}_N can be equivalently represented using Φ with a cancellation of the imaginary parts.

This imaginary-part cancellation effect does not generally hold when applying the matrix logarithm. Suppose the imaginary parts account for a significantly large value, the mutual representation of Φ and \mathcal{Z}_N does not match in the logarithmic scale. An exception holds unless the chosen dictionary is inherently rotation-free with respect to the true eigenfunctions [36], or there is direct access to the data for $\log(\mathcal{K}_\tau)$ allowing for direct training of the matrix. However, such conditions contravene our objective of leveraging Koopman data to conversely find the generator.

In comparison, the FDM and the resolvent-type approach approximate \mathcal{L} regardless of its boundedness. These two methods enable learning of L without computing the logarithm, thus avoiding the potential occurrence of imaginary parts caused by basis rotation. However, as we will see in Section VI, the performance of the FDM degrades as the sampling frequency decreases.

VI. CASE STUDIES

In this section, we test the effectiveness of the RTM method and compare its performance to the two benchmark methods, FDM and KLM. Particularly, we perform numerical examples for system identification of the following representative systems [33], [37]: the reversed Van der Pol oscillator (polynomial), two-machine power system (nonpolynomial), a system with rational vector fields (nonpolynomial), Lorenz-63 system (chaotic), and Lorenz-96 system (high-dimensional chaotic). We also show that the RTM is able to solve transport-related PDEs effectively. The research code can be found at <https://github.com/Yiming-Meng/Resolvent-Type-Learning-of-Koopman-Generators>.

We provide two measurements to demonstrate the error in system identification.

(1) The root mean squared error (RMSE) of flow

$$\mathcal{E}_{\text{RMSE}}^{\text{F}} = \frac{1}{M} \sum_{m=0}^{M-1} \sqrt{\frac{1}{\Gamma_s} \sum_{k=1}^{\Gamma_s} |\phi(t_k, x^{(m)}) - \hat{\phi}(t_k, x^{(m)})|^2} \quad (34)$$

measures the root mean square difference between the actual time-series data $\{\phi(t_k, x^{(m)})\}_{k=0}^{\Gamma_s}$ and the estimated data $\{\hat{\phi}(t_k, x^{(m)})\}_{k=0}^{\Gamma_s}$ using the learned generator up to time T_s . Here, Γ_s represents the number of snapshots used to verify the performance (which is independent of Γ , used for the data collection procedure), and the time $t_k = kT_s/\Gamma_s$ corresponds to the sampling instances.

(2) For polynomial models, and if we use monomial dictionary functions, we can use the RMSE of the weights assigned to each monomial

$$\mathcal{E}_{\text{RMSE}}^{\text{W}} := \sqrt{\frac{1}{dN} \sum_{j=1}^d \sum_{k=0}^{N-1} |\theta_k^j - \hat{\theta}_k^j|^2}. \quad (35)$$

Here, N represents the size the dictionary; d is the dimension of the system; θ_k^j is the weight for f_j at the k^{th} dictionary function; $\hat{\theta}_k^j$ is similarly defined but for the estimated vector field.

A. Reversed Van der Pol Oscillator

We use this example to thoroughly explain how the proposed method works and to highlight the phenomena discovered in the numerical example.

Consider the reversed Van der Pol oscillator

$$\dot{x}_1 = -x_2, \quad \dot{x}_2 = x_1 - (1 - x_1^2)x_2,$$

with $x := [x_1, x_2]$. We assume the system dynamics are unknown to us, and our information is limited to the system dimension, $d = 2$, and observations of sampled trajectories. To generate training data, we simply select $\Omega = (-1, 1)^2$ and obtain a total of $M = 10^2$ uniformly sampled initial conditions $\{x^{(m)}\}_{m=0}^{M-1}$ in Ω . We choose the dictionary as

$$\mathcal{Z}_N(x) = [\mathfrak{z}_0(x), \mathfrak{z}_1(x), \dots, \mathfrak{z}_{N-1}(x)], \quad N = P \times Q, \quad (36)$$

where $\mathfrak{z}_i(x) = x_1^p x_2^q$, $p = \text{mod}(i/P)$, and $q = \lfloor i/Q \rfloor$.

The actual vector field is $f(x) := [f_1(x), f_2(x)] = [-x_2, x_1 - (1 - x_1^2)x_2]$. As we can analytically establish that $\mathcal{L}_{\mathfrak{z}_1}(x) = [1, 0] \cdot f(x) = f_1(x)$ and $\mathcal{L}_{\mathfrak{z}_P}(x) = [0, 1] \cdot f(x) = f_2(x)$, by (24), we use the approximation $[\tilde{\mathcal{L}}_{\mathfrak{z}_1}, \tilde{\mathcal{L}}_{\mathfrak{z}_P}]$ to conversely obtain f .

To use the formula in Section V-C, we also need to determine the values of μ , λ , τ_s , and Γ . The discrete form $L (= L_{\text{mod}})$ can be then obtained according to Section V-C. We apply the learned L to identify the system vector fields. Note that $\mathfrak{z}_1(x) = \mathcal{Z}_N(x)\chi_1$ and $\mathfrak{z}_P(x) = \mathcal{Z}_N(x)\chi_P$, where each χ_i for $i \in \{0, 1, \dots, N-1\}$ is a column unit vector with all components being 0 except for the i -th component, which is 1. To apply L , we have that $\tilde{\mathcal{L}}_{\mathfrak{z}_1}(x) = \mathcal{Z}_N(x)(L\chi_1)$ and $\tilde{\mathcal{L}}_{\mathfrak{z}_P}(x) = \mathcal{Z}_N(x)(L\chi_P)$. In other words, we approximate

$\tilde{\mathcal{L}}_{\mathfrak{z}_1}$ and $\tilde{\mathcal{L}}_{\mathfrak{z}_P}$ (and hence f_1 and f_2) using a linear combination of functions within \mathcal{Z}_N .

1) *Test of Parameters of the RTM:* We first test how the parameters μ , λ , τ_s and Γ impact the precision of the RTM. As the impact of λ and τ_s has been shown analytically in Theorem 3.3 and 4.2, we can set λ to be a very large number while fixing τ_s to any reasonable value. The main focus of this part of the experiment is to see how tuning μ can impact performance under the constraint of Γ .

In the experiments, we set $\lambda = 1e8$ and $\tau_s = 5$, with $N = 3 \times 3$ monomials as in (36). We first use μ to evaluate the integral \mathcal{I}_μ under the sampling frequency 100 Hz (equivalently, $\Gamma = 500$), and then use (31) and (24) to learn the generator. Similarly, we perform the experiments for the cases of 50 Hz and 10 Hz. In Fig. 1, the relationship between τ_s , μ , and $\mathcal{E}_{\text{RMSE}}^{\text{W}}$ is illustrated.

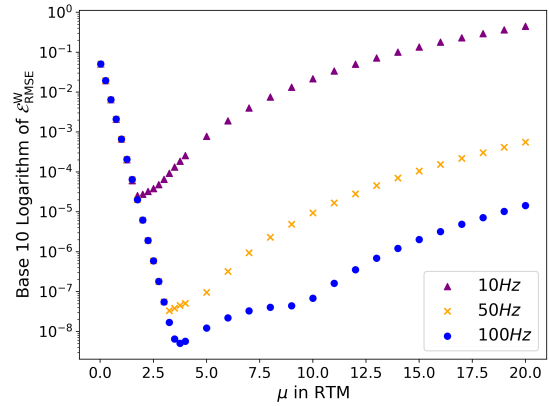


Fig. 1. RMSE of weights ($\mathcal{E}_{\text{RMSE}}^{\text{W}}$) using RTM for reversed Van der Pol oscillator with different sampling frequencies.

Under a sampling rate of 100 Hz, the highest accuracy ($\approx 10^{-8}$) is achieved at $\mu \approx 3.75$. A similar pattern is observed for the cases of 50 Hz and 10 Hz. However, the optimal accuracy decreases as the sampling frequency lowers, as expected. For a fixed tuple $(\tau_s, \lambda, \Gamma)$, it is clear that the accuracy of the numerical integral \mathcal{I}_μ increases as μ decreases, since the integrand $e^{-\mu s} \mathcal{K}_s \mathfrak{z}_i$ becomes less steep. By observing the form of the inference formula in (31) (or equivalently (41)), the non-monotonic trend of the learning accuracy with respect to changes in μ can be heuristically attributed to the combined effects of λ , μ , and the errors of the numerical integral.

Remark 6.1: A similar pattern has also been found in other numerical experiments, but we omit presenting them to avoid repetitive expression of the same idea. The optimal tuning of parameters can be roughly determined by the local Lipschitz constant of the system. It is of the authors' interest to pursue further numerical analysis to obtain a reasonable estimate of the tuning under mild assumptions about the system in future work.

The method has also been applied in real-world scenarios, such as identifying the car-following model [43], particularly in applications such as identifying the car-following model,

where the acceleration/deceleration (which directly determines the Lipschitz constant of the model) is known to be bounded. Numerical results provide a range for the choice of μ that leads to acceptable accuracy under other fixed parameters. \diamond

2) *Comparisons Among All Methods:* We compare the RTM with the FDM and KLM. We set $\mu = 3.25$ for RTM, while the other parameters remain the same as in the experiment in Section VI-A-1). The weights for these approximations are given by L_{χ_1} and L_{χ_3} , respectively. For better illustration, we report the results for all three methods under sampling rate $\gamma = 50$ Hz in Table I and II. The RMSE of weights ($\mathcal{E}_{\text{RMSE}}^{\text{W}}$) and the RMSE of flow ($\mathcal{E}_{\text{RMSE}}^{\text{F}}$) are reported in Table III for sampling rates of 10, 50, and 100 Hz.

The results demonstrate that the proposed resolvent-type method outperforms the other two benchmark methods overall. Particularly, the errors of FDM are at least 100 times higher than those of KLM and RTM at all tested sampling rates. The improvement in accuracy with increasing sampling rates for FDM is also not significant. A potential drawback of using the offline-learned dynamics by FDM is the requirement for more frequent resampling to ensure real-time operational safety.

On the other hand, KLM demonstrates a medium-level error compared to the others. One potential drawback of KLM is its sensitivity to the choice of dictionary functions, including the number and type of basis. In the preliminary version [39] of this paper, we showed that deliberately choosing different numbers for i and j (e.g. $N = 4 \times 3$) can lead to non-negligible imaginary parts after taking the matrix logarithm of K . A heuristic explanation can be found in Section V-D. The presence of these imaginary parts is significant and cannot be overlooked when aiming to minimize human intervention in identifying unknown systems in practice.

B. Scaled Lorenz-63 System

We consider the scaled Lorenz-63 system [44] by scaling it with a factor of ϵ , which yields

$$\begin{aligned} \dot{x}_1 &= \sigma(x_2 - \epsilon x_1), \\ \dot{x}_2 &= x_1(\gamma - x_3) - \epsilon x_2, \\ \dot{x}_3 &= x_1 x_2 - \epsilon \beta x_3, \end{aligned}$$

where $\sigma = 10$, $\gamma = 0.28$, $\beta = \frac{8}{3}$, and $\epsilon = 0.1$. With this so-called ϵ -Lorenz system, the system possesses an attractor on $\Omega = (-1, 1)^3$. We choose the dictionary of monomials with total number of $N = P \times Q \times J$ and set $\mathfrak{z}_i(x) = x_1^p x_2^q x_3^j$, where $p = i - PQj - Pq$, $q = \lfloor \frac{i - PQj}{P} \rfloor$, and $j = \lfloor \frac{i}{PQ} \rfloor$. Similar to Section VI-A, to identify the vector field, one can apply $\mathcal{L}_{\mathfrak{z}_1}$, $\mathcal{L}_{\mathfrak{z}_P}$, and $\mathcal{L}_{\mathfrak{z}_{P+Q}}$ after learning the generator.

The above scaled system is considered to facilitate easier observation within a smaller region of interest and to maintain a lower growth rate, ensuring that the tuning parameters remain within a reasonable range similar to the previous case study. Specifically, the original system (as studied in [33]) has the vector field $f(x) = [\sigma(x_2 - x_1), x_1(\gamma - x_3) - x_2, x_1 x_2 - \beta x_3]$, compared to the scaled version $f(x) = [\sigma(x_2 - \epsilon x_1), x_1(\gamma - x_3) - \epsilon x_2, x_1 x_2 - \epsilon \beta x_3]$.

Remark 6.2: Denoting the solution to the original Lorenz model as \hat{x} , it can be verified that $\hat{x}_1(t) = (1/\epsilon)x_1(\epsilon t)$,

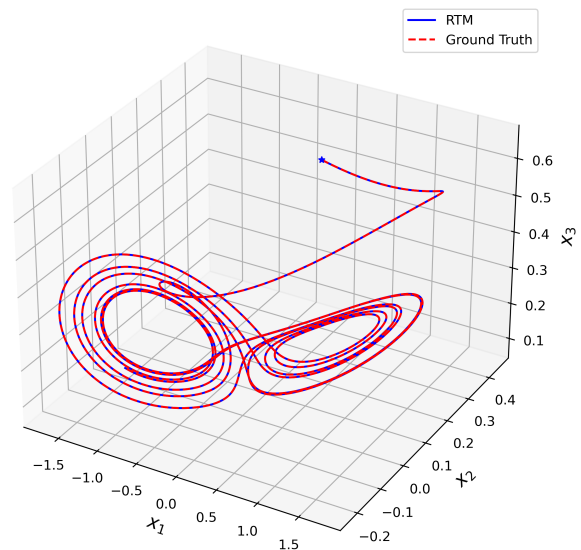


Fig. 2. Comparison of the trajectory using RTM with the ground truth for the scaled Lorenz-63 system, where the blue star denotes the initial condition.

$\hat{x}_2(t) = (1/\epsilon^2)x_2(\epsilon t)$, and $\hat{x}_3(t) = (1/\epsilon^2)x_3(\epsilon t)$. Let $\hat{\mathcal{L}}$ be the generator of the original system, one can also verify that $\hat{\mathcal{L}} = \epsilon \mathcal{L}$. It is worth noting that the scaling with $\epsilon > 0$ does not affect the topological stability. \diamond

In this case study, we set $P = Q = J = 2$ (or $N = 2^3$). We also set $\mu = 2$, $\lambda = 1e8$, and $\tau_s = 10$ for RTM. The comparisons for RMSE of weights and flow are summarized in Table III. Fig. 2 depicts the comparison of the trajectory for $T_s = 100$ using the approximated dynamics with RTM ($\gamma = 100$ Hz) and ground truth for an initial condition sampled in Ω , while the comparisons for the ones with KLM and FDM are included in Fig. 3. It is evident that the flow prediction using the dynamics approximated by RTM is highly accurate, successfully exhibiting the attractor (a long-term behavior) for this chaotic system, while the other two methods struggle to predict the trajectory effectively.

For chaotic systems, two trajectories starting very close together will rapidly diverge from each other, resulting in completely different long-term behaviors. The practical implication is that long-term prediction becomes impossible in such a system, where small errors are amplified extremely quickly. Such a two-point motion divergence phenomenon can be roughly characterized by the maximal Lyapunov exponent $\varrho > 0$ [45] and quantitatively expressed by $\mathcal{E}(t) \approx \mathcal{E}(0)e^{\varrho t}$, where the process $\{\mathcal{E}(t)\}_{t \geq 0}$ represents the evolution of error w.r.t. any initial condition. Suppose we now consider the original unscaled system (as studied in [33]), and denote $\hat{\mathcal{E}}(t)$ as the unscaled error. Then, in view of Remark 6.2 on the relation between the solutions of the original and scaled systems, one can obtain $|\hat{\mathcal{E}}(t/\epsilon)| \geq |\mathcal{E}(t)|/\epsilon$. Hence, whatever error is reflected in Fig. 2 and 3, the error for the unscaled version will be at least $1/\epsilon$ times larger at the extended time scale t/ϵ . For the prediction of a chaotic system, controlling the error within an even smaller tolerance level is necessary, and in this regard, RTM significantly outperforms the other two methods.

TABLE I
COMPARISONS OF THE WEIGHTS IN f_1 WITH THE GROUND TRUTH FOR REVERSED VAN DER POL OSCILLATOR WITH $\gamma = 50$

	1	x_1	x_1^2	x_2	$x_1 x_2$	$x_1^2 x_2$	x_2^2	$x_1 x_2^2$	$x_1^2 x_2^2$
Ground Truth	0	0	0	-1	0	0	0	0	0
FDM	2.89e-14	9.98e-3	-7.95e-14	-1 + 1.00e-2	-4.31e-15	-9.93e-3	-6.58e-14	1.32e-4	1.61e-13
KLM	2.92e-14	1.96e-8	-8.38e-14	-1 + 3.07e-8	-2.56e-15	1.18e-7	-8.21e-14	-1.79e-7	1.87e-13
RTM	-1.07e-16	1.03e-8	2.95e-16	-1 - 5.41e-8	-4.54e-16	-1.28e-8	-1.07e-16	3.28e-9	-7.69e-16

TABLE II
COMPARISONS OF THE WEIGHTS IN f_2 WITH THE GROUND TRUTH FOR REVERSED VAN DER POL OSCILLATOR WITH $\gamma = 50$

	1	x_1	x_1^2	x_2	$x_1 x_2$	$x_1^2 x_2$	x_2^2	$x_1 x_2^2$	$x_1^2 x_2^2$
Ground Truth	0	1	0	-1	0	1	0	0	0
FDM	2.46e-14	1 - 2.82e-3	-3.23e-14	-1 - 1.00e-3	-1.23e-15	1 - 1.03e-2	-4.77e-14	-1.98e-2	5.64e-14
KLM	2.44e-14	1 - 4.16e-7	-4.91e-14	-1 - 2.26e-5	-2.42e-15	1 + 9.53e-5	-3.98e-14	3.09e-5	5.33e-14
RTM	-4.57e-16	1 + 4.66e-8	6.47e-16	-1 - 8.07e-8	-1.71e-16	1 + 5.79e-8	8.68e-16	6.69e-8	-1.60e-15

TABLE III
COMPARISONS OF RMSE OF WEIGHTS AND FLOW OVER 100 TRAJECTORIES FOR THE THREE POLYNOMIAL SYSTEMS

System	M	N	Sampling Rate γ (Hz)	RMSE of weights ($\mathcal{E}_{\text{RMSE}}^W$)			RMSE of flow ($\mathcal{E}_{\text{RMSE}}^F$)		
				FDM	KLM	RTM	FDM	KLM	RTM
Reversed Van der Pol	10^2	9	10	3.36e-2	5.91e-4	9.24e-5	3.21e-2	1.51e-4	1.26e-4
			50	6.70e-3	2.42e-5	3.31e-8	7.02e-3	6.27e-6	3.82e-8
			100	3.35e-3	6.74e-6	1.70e-8	3.54e-3	1.73e-6	1.86e-8
Scaled Lorenz-63 (3-dimensional)	20^3	8	10	1.82e-1	6.98e-3	5.78e-4	6.15e-1	3.52e-2	3.54e-3
			50	3.81e-2	2.87e-4	1.44e-7	3.43e-1	1.60e-3	1.61e-6
			100	1.92e-2	7.17e-5	2.40e-8	2.27e-1	4.35e-4	7.45e-8
Lorenz-96 (6-dimensional)	10^6	64	10	2.18e-2	3.08e-4	4.75e-5	2.15e-2	3.61e-4	1.37e-4
			50	4.61e-3	1.21e-5	6.08e-8	4.40e-3	1.57e-5	1.25e-7
			100	2.32e-3	3.03e-6	5.37e-9	2.20e-3	3.97e-6	1.54e-8

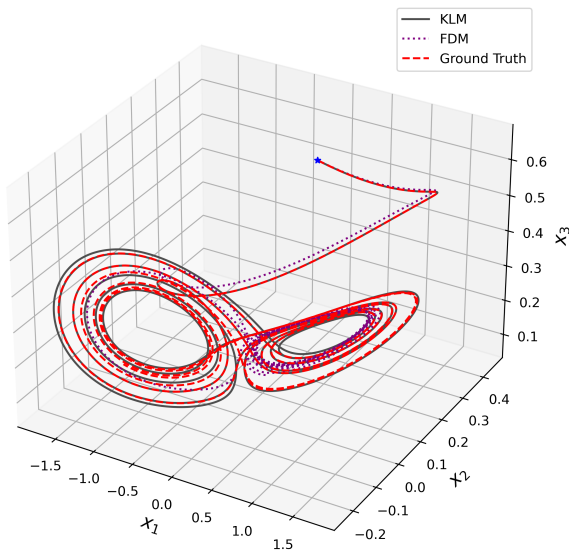


Fig. 3. Comparison of the trajectories using KLM and FDM with the ground truth for the scaled Lorenz-63 system, where the blue star denotes the initial condition.

C. Lorenz-96 System

In this case study, we work on a high-dimensional chaotic system, the monoscale Lorenz-96 system [46], given as

$$\dot{x}_j = -x_{j-2}x_{j-1} + x_{j-1}x_{j+1} - x_j + F$$

for all $j \in \{1, 2, \dots, d\}$. Here, we set $d = 6$ and $F = 0.1$ with $\Omega = (-1, 1)^d$, such that the forward invariance w.r.t. Ω can be guaranteed. Considering that this is a high-dimensional system, we simply set the number of monomials in the dictionary to $N = 2^d$, using a similar indexing method as in the previous case studies.

For RTM, we set $\tau_s = 4$, $\lambda = 1e8$ and set $\mu = 2, 4, 5$ for 10, 50, 100 Hz sampling rates, respectively. The detailed comparisons with the other two methods are listed in Table III.

As shown in the table, for all three polynomial systems (Section VI-A to VI-C), RTM reaches better accuracy in terms of the errors for both the weights and the flow. In addition, all three methods show better performance as the sampling rate increases when using the monomial dictionary functions, with FDM exhibiting the slowest rate of improvement.

For non-polynomial systems, selecting monomial dictionary functions may be ineffective due to their limited expressiveness. To enhance adaptability in characterizing the generator for more general dynamical systems, we will continue to investigate the impact of using non-polynomial dictionary functions for all three methods in the upcoming experiments.

D. Two-Machine Power System

Consider the two-machine power system [6] modelled by

$$\dot{x}_1 = x_2, \quad \dot{x}_2 = -0.5x_2 - (\sin(x_1 + \zeta) - \sin(\zeta)),$$

where $\zeta = \frac{\pi}{3}$. Since the vector field consists of polynomial and periodic terms, using monomial approximations appears

to be local and may not be satisfactory. Instead, we utilize the less biased hidden layers of random feature neural networks as the dictionary functions.

Remark 6.3 (Related Work): In the context of Koopman operator learning, the authors of [47] proposed a consistent Koopman autoencoder neural network structure aimed at achieving better approximation performance. Essentially, this autoencoder seeks to find the $K = \operatorname{argmin}_{A \in \mathbb{C}^{N \times N}} \|Z - XA\|_F$ by optimally matching the input and output data. However, for deep neural network-based dictionary functions, a closed-form expression cannot be obtained, as they are not linear combinations. Additionally, the training process tends to be computationally expensive.

Comparatively, the work in [48] demonstrates that shallow tanh neural networks suffice to approximate functions at comparable or better rates than much deeper ReLU neural networks. The approximation error decreases when the number of hidden neurons increases [48]. Numerous applications have also been explored in solving first-order linear PDEs, highlighting their expressive power.

In the upcoming experiments, we leverage this expressive feature by using shallow tanh-activated neural networks as the dictionary functions, achieving the linear combination effect of the test and image functions of the learned operator. \diamond

By choosing tanh as the activation function, the dictionary of observable functions mainly consists of $\tanh(xW^T + b^T)$, where $W \in \mathbb{R}^{\sigma \times n}$ and $b \in \mathbb{R}^{\sigma}$ are the randomly generated weight and bias of the first layer, respectively, and tanh is applied elementwise. To obtain the expressions of the vector fields, we also need to add $\{x_j\}_{j=1}^d$ to the dictionary (recall that $\mathcal{L}x_j = f_j$). All together, the dictionary $\mathcal{Z}_N(x)$ consists of σ random feature neural networks appended by $\{x_j\}_{j=1}^d$, with a total of $N = \sigma + n$ elements.

We sampled $M = 150^2$ initial points uniformly across $\Omega = (-1, 1)^2$ with $\tau_s = 5$. For RTM, we set $\lambda = 1e8$ and $\mu = 2$ for all sampling frequencies. As we cannot compare the RMSE of weights in this case, the comparisons of RMSE of flow with three different frequencies are summarized in Table IV. Like polynomial systems, RTM outperforms the other two methods.

Particularly, as with the tanh neural networks, the learned Koopman matrix K does not preserve the diagonal property, leading to non-negligible imaginary parts after taking the matrix logarithm of K . The RMSE of the imaginary parts of flow using KLM is reported in Appendix C.

The trajectories generated with the approximated dynamics for all three methods are close to the ground truth when $\sigma = 50$ with $\tau = 0.01$. However, when σ increases to 100, both the performances of FDM and KLM deteriorate, especially KLM, as shown in Fig. 4. These results validate the statement that when one lacks prior knowledge of the underlying system, which makes it difficult to determine the number and/or types of dictionary functions, both FDM and KLM may struggle to produce accurate results in system identification.

E. Nonpolynomial Vector Fields

Consider a system with nonpolynomial vector fields:

$$\dot{x}_1 = -x_1 + \frac{4x_2}{1+x_2^2}, \quad \dot{x}_2 = -x_2 - \frac{4x_1}{1+x_2^2}.$$

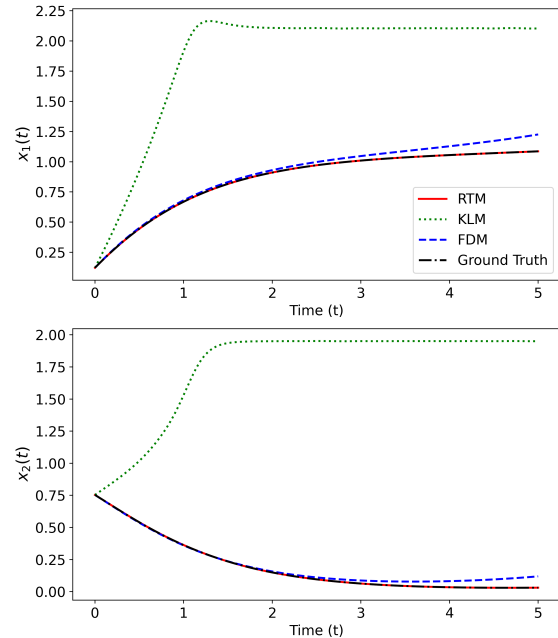


Fig. 4. Comparisons of the trajectories with the approximated dynamics using three different methods and ground truth for the two-machine power system.

TABLE IV
COMPARISONS OF RMSE OF FLOW OVER 100 TRAJECTORIES FOR THE TWO-MACHINE POWER SYSTEM

System	N	Sampling Rate (Hz)	RMSE of flow ($\mathcal{E}_{\text{RMSE}}^F$)		
			FDM	KLM	RTM
Two-machine	22	10	6.63	3.67	1.52e-1
		50	5.67	5.14	1.61e-1
		100	4.43	4.23	1.33e-1
Two-machine	52	10	1.80e-1	1.35e-1	5.23e-2
		50	1.35e-1	1.29e-1	4.76e-2
		100	8.54e-2	8.51e-2	2.44e-2
Two-machine	102	10	3.33e-2	1.83e-1	6.06e-3
		50	8.56e-2	1.14	6.06e-3
		100	1.90e-1	3.00	9.55e-2

For this nonpolynomial system, as shown in [36], it is necessary to include $\{\frac{x_i}{1+x_j^2}\}$ in the dictionary functions for the exact identification of the model. However, this prior knowledge is typically not accessible for most nonlinear systems in practice. To reduce the bias in selecting dictionary functions, we continue to use random feature NNs as the dictionary functions. Regrading training data, $M = 100^2$ initial points are uniformly sampled within $\Omega = (-1, 1)^2$. We also set $\tau_s = 5$ and $\lambda = 1e8$ for RTM.

As discussed in Section VI-A, the choice of μ has impacts on the accuracy of the results for RTM. We set $\mu = 0.5, 2, 2$ for the cases of $\sigma = 20, 50, 100$, respectively, to achieve near-optimal performance. The comparisons are detailed in Table V. It is worth noting that when $\sigma = 100$ and $\tau = 0.1$, KLM fails to return meaningful results, as the trajectory of the approximated dynamics blows up.

TABLE V
COMPARISONS OF RMSE OF FLOW OVER 100 TRAJECTORIES FOR THE
NONPOLYNOMIAL SYSTEM

System	N	Sampling Rate (Hz)	RMSE of flow ($\mathcal{E}_{\text{RMSE}}^{\text{F}}$)		
			FDM	KLM	RTM
Nonpoly ($\mu = 0.5$)	22	10	7.43e-2	2.96e-3	1.49e-3
		50	1.92e-2	2.20e-3	1.35e-3
		100	1.03e-2	2.30e-3	1.48e-3
Nonpoly ($\mu = 2$)	52	10	7.72e-2	2.71e-1	7.62e-4
		50	2.04e-2	3.11e-2	2.40e-4
		100	1.11e-2	2.43e-2	2.40e-4
Nonpoly ($\mu = 2$)	102	10	7.22e-2	-	5.88e-4
		50	2.13e-2	2.83e-1	1.35e-5
		100	2.52e-2	1.71e-1	8.68e-5

F. Prediction of Region of Attraction

In this subsection, we demonstrate that both the dataset and dictionary functions can be reused to predict the region of attraction (RoA) \mathcal{D} of an equilibrium point x_{eq} for the system⁴. For simplicity, we can assume that the system has an equilibrium point at the origin.

The methodology involves using the learned generator to solve a Zubov's equation of the form

$$\mathcal{L}u(x) = -\alpha|x - x_{\text{eq}}|^2(1 - u(x)), \quad \alpha > 0. \quad (37)$$

The solution should have the following properties: 1) $0 < u(x) < 1$ for all $x \in \mathcal{D} \setminus \{x_{\text{eq}}\}$, and 2) $u(x) \rightarrow 1$ as $x \rightarrow y$ for any $y \in \partial\mathcal{D}$. Therefore, the set $\{x \in \mathbb{R}^n : u(x) < 1\}$ can readily represent the RoA. Moreover, for any approximator \tilde{u} of u such that $|\tilde{u} - u|_{\infty} \leq \varepsilon$, one can show that the set $\{x : \tilde{u}(x) \leq 1 - \varepsilon\}$ is a tight inner approximation of the RoA.

Remark 6.4: Note that the RoA can also be characterized by the function domain D of a maximal Lyapunov function v if the following conditions hold: 1) $v(x_{\text{eq}}) = 0$ and $v(x) > 0$ for all $x \in D \setminus \{x_{\text{eq}}\}$; 2) the derivative of v along solutions of (1) is well-defined for all $x \in D$ and satisfies the Lyapunov equation

$$\mathcal{L}v(x) = -|x - x_{\text{eq}}|^2; \quad (38)$$

and 3) $v(x) \rightarrow \infty$ as $x \rightarrow \partial D$ or $|x| \rightarrow \infty$.

It can be verified that $u(x) = 1 - \exp(-\alpha v(x))$ for all $x \in \mathcal{D}(\mathcal{A})$, and $u(x) = 1$ elsewhere, is the unique bounded viscosity solution that satisfies the required properties [49]. We prefer to use u instead of v for characterizing the RoA due to its global boundedness, which allows the extension of the function domain to the entire state space or any desired set where computations take place. Additional features of the above PDEs can be found in [49], [50]. \diamond

To illustrate the accuracy of the learned generator, as well as the effectiveness of using it to solve Eq. (37), we revisit the reversed Van der Pol oscillator system. The difference is that we choose the dictionary $\mathcal{Z}_N(x)$ the same as in Sections VI-D and VI-E, which consists of the σ -dimensional random feature neural network $\tanh(xW^{\text{T}} + b^{\text{T}})$ appended with $\{x_1, x_2\}$. In the experiment, we set $\sigma = 100$, $\mu = 10$, and $M = 100^2$.

With the above settings, we can achieve a good approximation of the dynamics with the RMSE of flow $\mathcal{E}_{\text{RMSE}}^{\text{F}}$

$= 1.08e-5$. We find an approximate equilibrium point at $[6.81e-8, -1.25e-8]$, which is sufficiently close to the origin with negligible error. In addition, we observe that the average approximation error of $\mathcal{L} \tanh(xW^{\text{T}} + b^{\text{T}})$ is $1.66e-4$, indicating an overall good performance of the least-squares regression L .

We aim to find a single-hidden-layer feedforward neural network of the form $u(x; \theta) = \mathcal{Z}_N(x)\theta$ that approximates the unique bounded viscosity solution of $\mathcal{L}u(x) = -\alpha|x|^2(1 - u(x))$ with $\alpha = 0.1$ and the boundary condition $V(\mathbf{0}) = 0$. Due to the fact that $\nabla u(x; \theta) \cdot \tilde{f}(x) \approx \mathcal{L}u(x; \theta) \approx \mathcal{Z}_N(x)L\theta$ for all $u(x; \theta) = \mathcal{Z}_N(x)\theta$, where $\tilde{f}(x)$ is the approximated vector field using the learned generator, it is equivalent to finding the weights θ that approximately satisfy

$$\mathcal{Z}_N(x)L\theta = -\alpha|x|^2(1 - u(x; \theta)) \quad (39)$$

or

$$\nabla u(x; \theta) \cdot \tilde{f}(x) = -\alpha|x|^2(1 - u(x; \theta)), \quad (40)$$

ensuring that $u(x; \theta)$ is bounded and a viscosity solution at the same time.

It is worth noting that, without the boundary condition and the constraints on its viscosity property, the problem can be reduced to finding the θ that minimizes the least-squares error (residual loss) between the l.h.s. and r.h.s. of Eq. (39) (or (40)) at those sampled initial conditions. However, such a solution may not possess the correct physical meaning, with a simple counterexample being $u(x; \theta) \approx 1$ for all x .

Inspired by recent research on physics-informed neural networks, it is also necessary to introduce and minimize additional loss terms, beyond the residual loss, that encompass the PDE and any supplementary information pertinent to the problem [49], [51], [52]. In this case, we specifically need to consider loss terms to match the condition $u(\mathbf{0}; \theta) = 0$ and valued on $\partial\Omega$. Clearly, finding θ that minimizes the weighted sum of these loss terms does not have a closed-form solution. That said, an extreme learning machine (ELM), which seeks solutions of the form $\mathcal{Z}_N(x)\theta$ for PDEs that are linear in both u and ∇u , transforms the optimization into a linear least-squares problem that can be efficiently solved, exhibiting fast learning speed and strong generalization performance [52].

Based on the above feature, and for the purpose of obtaining a valid physics-informed approximation of $u(x)$ with efficient computation, we can leverage the well-tuned toolbox LyZNet [51] to implement the physics-informed ELM algorithm. The learned Lyapunov function and the corresponding region of attraction estimate can be found in Fig. 5, where the blue curve represents the region of attraction estimate, which is sufficiently close to the true region of attraction.

Remark 6.5: As investigated in [52], one can expect good performance from using random feature neural networks to solve transport-related PDEs that are linear in u and ∇u . The key lies in the ability of using weighted $\tanh(xW^{\text{T}} + b^{\text{T}})$ to approximate $u(x)$, $\mathcal{L}u(x)$, and $f(x)$, as well as the accuracy of the learned L that guarantees $\nabla u(x; \theta) \cdot \tilde{f}(x) \approx \mathcal{L}u(x; \theta) \approx \mathcal{Z}_N(x)L\theta$.

Other dictionary functions may have the above features. However, the choice may depend on side information and

⁴Supposing that x_{eq} is asymptotically stable, the RoA of x_{eq} is a set defined as $\mathcal{D} := \{x \in \Omega : \lim_{t \rightarrow \infty} |\phi(t, x) - x_{\text{eq}}| = 0\}$.

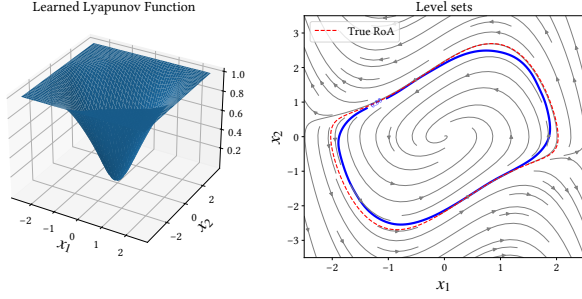


Fig. 5. Learned Lyapunov function and the corresponding region of attraction estimate using the random feature neural network dictionary functions for the reversed Van der Pol oscillator.

the solution space properties, which is not conducive to data-driven approximation for unknown systems. \diamond

VII. CONCLUSION

In this paper, we propose a novel resolvent-type Koopman operator-based learning framework for the generator of unknown systems. The proposed method demonstrates both theoretical and numerical improvements over the Koopman logarithm method [33] and the finite difference method [28], offering greater adaptability in handling low observation rate scenarios and utilizing less biased random feature neural networks as dictionary functions. Specifically, in cases where the logarithm of the Koopman operator is invalid for representing the generator, we draw upon the rich literature to propose data-driven approximations based on Yosida's approximation and the properties of the resolvent operator. The analytical convergence rate and a modified data-driven learning algorithm are provided to assist users in tuning the parameters.

The current drawbacks lie in tuning the parameter μ under the constraints of the observation rate, as well as in the lack of understanding regarding the sampling efficiency of the initial conditions. We will pursue these analyses in future work and provide a more systematic and automated parameter tuning strategy, with the ultimate goal of developing a software toolbox for data-driven system verification of unknown systems. We also expect that the current research and the analysis of data efficiency will lay the foundations for studying control systems, shed light on dimension reduction in generator learning, and be beneficial for developing an online learning adaptation of this method with a provable error bound. Another possible extension direction based on the current research is robustness analysis under noisy and partial observations.

APPENDIX A

PROOFS IN TECHNICAL RESULTS

Proof of Proposition 3.5: For all $h \in \mathcal{C}^1(\Omega)$ and $x \in \Omega$, we have

$$\begin{aligned}
 & \mathcal{R}(\lambda)(\lambda \text{Id} - \mathcal{L})h(x) \\
 &= \lambda \mathcal{R}(\lambda)h(x) - \mathcal{R}(\lambda)\mathcal{L}h(x) \\
 &= \lambda \int_0^\infty e^{-\lambda t} h(\phi(t, x)) dt - \int_0^\infty e^{-\lambda t} \mathcal{L}h(\phi(t, x)) dt \\
 &= -h(\phi(t, x))e^{-\lambda t} \Big|_0^\infty + \int_0^\infty e^{-\lambda t} d(h(\phi(t, x))) \\
 &\quad - \int_0^\infty e^{-\lambda t} \mathcal{L}h(\phi(t, x)) dt \\
 &= h(\phi(0, x)) = h(x),
 \end{aligned}$$

where we have used the fact that the time derivative along the trajectories of (1) is such that $dh(x)/dt = \mathcal{L}h(x)$.

On the other hand, for all $h \in \mathcal{C}(\Omega)$, all $x \in \Omega$, and all $t \geq 0$,

$$\begin{aligned}
 & \mathcal{R}(\lambda)h(x) \\
 &= \int_0^t \mathcal{K}_{s, -\lambda} h(x) ds + \int_t^\infty \mathcal{K}_{s, -\lambda} h(x) ds \\
 &= \int_0^t \mathcal{K}_{s, -\lambda} h(x) ds + \int_0^\infty \mathcal{K}_{t+s, -\lambda} h(x) ds \\
 &= \int_0^t e^{-\lambda s} \mathcal{K}_s h(x) ds + e^{-\lambda t} \mathcal{R}(\lambda)h(\phi(t, x)).
 \end{aligned}$$

However,

$$\mathcal{K}_t \mathcal{R}(\lambda)h(x) = \int_0^\infty e^{-\lambda s} \mathcal{K}_s h(\phi(t, x)) ds = \mathcal{R}(\lambda) \mathcal{K}_t h(x).$$

Therefore,

$$\begin{aligned}
 & \frac{\mathcal{K}_t \mathcal{R}(\lambda)h(x) - \mathcal{R}(\lambda)h(x)}{t} \\
 &= \frac{\mathcal{K}_t \mathcal{R}(\lambda)h(x) - e^{-\lambda t} \mathcal{R}(\lambda)h(\phi(t, x))}{t} \\
 &\quad + \frac{e^{-\lambda t} \mathcal{R}(\lambda)h(\phi(t, x)) - \mathcal{R}(\lambda)h(x)}{t} \\
 &= \frac{\mathcal{K}_t \mathcal{R}(\lambda)h(x) - e^{-\lambda t} \mathcal{K}_t \mathcal{R}(\lambda)h(x)}{t} - \frac{1}{t} \int_0^t e^{-\lambda s} \mathcal{K}_s h(x) ds.
 \end{aligned}$$

With $t \downarrow 0$ on both sides, we have $\mathcal{L} \mathcal{R}(\lambda)h(x) = \lambda \mathcal{R}(\lambda)h(x) - h(x)$, which is equivalent as $(\lambda \text{Id} - \mathcal{L}) \mathcal{R}(\lambda)h(x) = h(x)$. \blacksquare

Proof of Corollary 4.6: We show the sketch of the proof. Working on the compact family of $\{\mathcal{K}_s^\varepsilon\}_{s \in (0, \tau_s]}$ for some small $\varepsilon > 0$, one can find a sufficiently large N such that

$$|\mathcal{K}_s^N h - \mathcal{K}_s h|_\infty < \delta, \quad h \in \mathcal{C}(\Omega), \quad s \in (0, \tau_s],$$

where K_s^N is the finite-dimensional representation of K_s^ε . Let $\mathcal{R}_{\lambda, \tau_s}^N := \int_0^{\tau_s} e^{-\lambda s} \mathcal{K}_s^N ds$. Then, for any $t \in (0, \tau_s)$,

$$\begin{aligned}
 & |\mathcal{R}_{\lambda, \tau_s}^N h - \mathcal{R}_{\lambda, \tau_s} h|_\infty \\
 &\leq \int_0^t e^{-\lambda s} |\mathcal{K}_s^N h - \mathcal{K}_s h|_\infty ds + \int_t^{\tau_s} e^{-\lambda s} |\mathcal{K}_s^N h - \mathcal{K}_s h|_\infty ds \\
 &\leq C|h|_\infty t + \sup_{s \in (0, \tau_s]} |\mathcal{K}_s^N h - \mathcal{K}_s h|_\infty \cdot \frac{e^{-\lambda t} - e^{-\lambda \tau_s}}{\lambda} \\
 &< C|h|_\infty t + \delta,
 \end{aligned}$$

where $C := \sup_{s \in (0, t]} \|K_s^N\| + C e^{\omega t}$. The conclusion follows by sending $t \rightarrow 0$. \blacksquare

APPENDIX B
MODIFIED GENERATOR LEARNING FORMULA

We derive the modified formula for L_{mod} in Section V-C. For any $h \in \mathcal{C}^1(\Omega)$, by the first resolvent identity (30), we have

$$\begin{aligned} & [(\lambda - \mu)\mathcal{R}(\mu) + \text{Id}](\lambda^2\mathcal{R}(\lambda)h(x) - \lambda h(x) + \lambda h(x)) \\ &= \lambda^2\mathcal{R}(\mu)h(x). \end{aligned}$$

Then,

$$[(\lambda - \mu)\mathcal{R}(\mu) + \text{Id}](\mathcal{L}_\lambda h(x) + \lambda h(x)) = \lambda^2\mathcal{R}(\mu)h(x),$$

and

$$\begin{aligned} & \mathcal{L}_\lambda[(\lambda - \mu)\mathcal{R}(\mu) + \text{Id}]h(x) \\ &= \lambda^2\mathcal{R}(\mu)h(x) - \lambda(\lambda - \mu)\mathcal{R}(\mu)h(x) - \lambda h(x) \\ &= \lambda\mu\mathcal{R}(\mu)h(x) - \lambda h(x), \end{aligned}$$

where we have used the commutativity of \mathcal{L} (or \mathcal{L}_λ) and its resolvent. Letting $\tilde{\mathcal{I}} := \mu^2\mathcal{R}(\mu)$, then,

$$\mathcal{L}_\lambda \left[\frac{\lambda - \mu}{\mu^2} \tilde{\mathcal{I}} + \text{Id} \right] h(x) = \left[\frac{\lambda}{\mu} \tilde{\mathcal{I}} - \lambda \text{Id} \right] h(x). \quad (41)$$

It is also clear that, in a strong sense, $\mathcal{L} \left[\frac{\lambda - \mu}{\mu^2} \tilde{\mathcal{I}} + \text{Id} \right] h(x) \approx \left[\frac{\lambda}{\mu} \tilde{\mathcal{I}} - \lambda \text{Id} \right] h(x)$. We then solve this equation using a data-fitting method.

Recall notation in (32). One can obtain the fully discretized version of the operator $\frac{\lambda - \mu}{\mu^2} \tilde{\mathcal{I}} + \text{Id}$ in a similar way as in Section V-B, as $(X^\top X)^\dagger X^\top A$. Similarly, the fully discretized version of the operator $\frac{\lambda}{\mu} \tilde{\mathcal{I}} - \lambda \text{Id}$ is $(X^\top X)^\dagger X^\top B$. It can be shown that the data-driven version of (41) is such that $\mathcal{Z}_N(\cdot) (X^\top X)^\dagger X^\top A(L_{\text{mod}}\theta) \approx \mathcal{Z}_N(\cdot) (X^\top X)^\dagger X^\top B\theta$. Solving it in the least squares sense gives the formula (32).

APPENDIX C
SUPPLEMENTARY RESULTS IN SECTION VI

We present the RMSE of the imaginary parts of flow using KLM for the two-machine power system in Section VI-D. The results are reported in Table VI.

TABLE VI
RMSE OF THE IMAGINARY PARTS OF FLOW OVER 100 TRAJECTORIES FOR THE TWO-MACHINE POWER SYSTEM USING KLM

System	N	Sampling Rate (Hz)	RMSE of imaginary part
Two-machine	22	10	0.99
		50	1.02
		100	0.10
Two-machine	52	10	1.10
		50	1.09
		100	0.98
Two-machine	102	10	0.82
		50	0.84
		100	0.551

REFERENCES

- [1] S. N. Ethier and T. G. Kurtz, *Markov Processes: Characterization and Convergence*. John Wiley & Sons, 2009.
- [2] B. O. Koopman, "Hamiltonian systems and transformation in Hilbert space," *Proceedings of the National Academy of Sciences*, vol. 17, no. 5, pp. 315–318, 1931.
- [3] M. Reed and B. Simon, *Methods of Modern Mathematical Physics: Functional Analysis*, vol. 1. Gulf Professional Publishing, 1980.
- [4] G. A. Pavliotis and A. Stuart, *Multiscale Methods: Averaging and Homogenization*, vol. 53. Springer Science & Business Media, 2008.
- [5] L. C. Evans, *Partial Differential Equations*, vol. 19. American Mathematical Society, 2022.
- [6] A. Vannelli and M. Vidyasagar, "Maximal Lyapunov functions and domains of attraction for autonomous nonlinear systems," *Automatica*, vol. 21, no. 1, pp. 69–80, 1985.
- [7] I. M. Mitchell, A. M. Bayen, and C. J. Tomlin, "A time-dependent Hamilton-Jacobi formulation of reachable sets for continuous dynamic games," *IEEE Transactions on Automatic Control*, vol. 50, no. 7, pp. 947–957, 2005.
- [8] M. Bardi and I. C. Dolcetta, *Optimal Control and Viscosity Solutions of Hamilton-Jacobi-Bellman Equations*, vol. 12. Springer, 1997.
- [9] M. G. Crandall and P.-L. Lions, "Viscosity solutions of Hamilton-Jacobi equations," *Transactions of the American mathematical society*, vol. 277, no. 1, pp. 1–42, 1983.
- [10] J. Sjöberg, Q. Zhang, L. Ljung, A. Benveniste, B. Delyon, P.-Y. Glorennec, H. Hjalmarsson, and A. Juditsky, "Nonlinear black-box modeling in system identification: a unified overview," *Automatica*, vol. 31, no. 12, pp. 1691–1724, 1995.
- [11] R. Haber and H. Unbehauen, "Structure identification of nonlinear dynamic systems—a survey on input/output approaches," *Automatica*, vol. 26, no. 4, pp. 651–677, 1990.
- [12] Y. Lin, E. D. Sontag, and Y. Wang, "A smooth converse Lyapunov theorem for robust stability," *SIAM Journal on Control and Optimization*, vol. 34, no. 1, pp. 124–160, 1996.
- [13] A. R. Teel and L. Praly, "A smooth Lyapunov function from a class-estimate involving two positive semidefinite functions," *ESAIM: Control, Optimisation and Calculus of Variations*, vol. 5, pp. 313–367, 2000.
- [14] Y. Meng, Y. Li, M. Fitzsimmons, and J. Liu, "Smooth converse Lyapunov-barrier theorems for asymptotic stability with safety constraints and reach-avoid-stay specifications," *Automatica*, vol. 144, p. 110478, 2022.
- [15] A. D. Ames, X. Xu, J. W. Grizzle, and P. Tabuada, "Control barrier function based quadratic programs for safety critical systems," *IEEE Transactions on Automatic Control*, vol. 62, no. 8, pp. 3861–3876, 2016.
- [16] A. D. Ames, S. Coogan, M. Egerstedt, G. Notomista, K. Sreenath, and P. Tabuada, "Control barrier functions: Theory and applications," in *2019 18th European Control Conference (ECC)*, pp. 3420–3431, IEEE, 2019.
- [17] Y. Meng and J. Liu, "Lyapunov-barrier characterization of robust reach-avoid-stay specifications for hybrid systems," *Nonlinear Analysis: Hybrid Systems*, vol. 49, p. 101340, 2023.
- [18] I. Mezić, "Spectral properties of dynamical systems, model reduction and decompositions," *Nonlinear Dynamics*, vol. 41, pp. 309–325, 2005.
- [19] W. Pan, Y. Yuan, J. Gonçalves, and G.-B. Stan, "A sparse Bayesian approach to the identification of nonlinear state-space systems," *IEEE Transactions on Automatic Control*, vol. 61, no. 1, pp. 182–187, 2015.
- [20] S. L. Brunton, J. L. Proctor, and J. N. Kutz, "Discovering governing equations from data by sparse identification of nonlinear dynamical systems," *Proceedings of the National Academy of Sciences*, vol. 113, no. 15, pp. 3932–3937, 2016.
- [21] J. C. Nash and M. Walker-Smith, "Nonlinear parameter estimation," *An integrated system on BASIC*. NY, Basel, vol. 493, 1987.
- [22] J. M. Varah, "A spline least squares method for numerical parameter estimation in differential equations," *SIAM Journal on Scientific and Statistical Computing*, vol. 3, no. 1, pp. 28–46, 1982.
- [23] S. E. Otto and C. W. Rowley, "Koopman operators for estimation and control of dynamical systems," *Annual Review of Control, Robotics, and Autonomous Systems*, vol. 4, no. 1, pp. 59–87, 2021.
- [24] A. Mauroy and I. Mezić, "A spectral operator-theoretic framework for global stability," in *52nd IEEE Conference on Decision and Control*, pp. 5234–5239, IEEE, 2013.
- [25] A. Mauroy and I. Mezić, "Global stability analysis using the eigenfunctions of the Koopman operator," *IEEE Transactions on Automatic Control*, vol. 61, no. 11, pp. 3356–3369, 2016.
- [26] S. A. Deka, A. M. Valle, and C. J. Tomlin, "Koopman-based neural Lyapunov functions for general attractors," in *61st Conference on Decision and Control (CDC)*, pp. 5123–5128, IEEE, 2022.

- [27] Y. Meng, R. Zhou, and J. Liu, "Learning regions of attraction in unknown dynamical systems via Zubov-Koopman lifting: Regularities and convergence," *arXiv preprint arXiv:2311.15119*, 2023.
- [28] J. J. Bramburger and G. Fantuzzi, "Auxiliary functions as Koopman observables: Data-driven analysis of dynamical systems via polynomial optimization," *Journal of Nonlinear Science*, vol. 34, no. 1, p. 8, 2024.
- [29] S. Klus, F. Nüske, S. Peitz, J.-H. Niemann, C. Clementi, and C. Schütte, "Data-driven approximation of the Koopman generator: Model reduction, system identification, and control," *Physica D: Nonlinear Phenomena*, vol. 406, p. 132416, 2020.
- [30] A. Nejati, A. Lavaei, S. Soudjani, and M. Zamani, "Data-driven estimation of infinitesimal generators of stochastic systems," *IFAC-PapersOnLine*, vol. 54, no. 5, pp. 277–282, 2021.
- [31] C. Wang, Y. Meng, S. L. Smith, and J. Liu, "Data-driven learning of safety-critical control with stochastic control barrier functions," in *61st Conference on Decision and Control (CDC)*, pp. 5309–5315, IEEE, 2022.
- [32] S. Otto, S. Peitz, and C. Rowley, "Learning bilinear models of actuated koopman generators from partially observed trajectories," *SIAM Journal on Applied Dynamical Systems*, vol. 23, no. 1, pp. 885–923, 2024.
- [33] A. Mauroy and J. Goncalves, "Koopman-based lifting techniques for nonlinear systems identification," *IEEE Transactions on Automatic Control*, vol. 65, no. 6, pp. 2550–2565, 2019.
- [34] Z. Drmač, I. Mezić, and R. Mohr, "Identification of nonlinear systems using the infinitesimal generator of the Koopman semigroup—a numerical implementation of the Mauroy–Goncalves method," *Mathematics*, vol. 9, no. 17, p. 2075, 2021.
- [35] M. Black and D. Panagou, "Safe control design for unknown nonlinear systems with Koopman-based fixed-time identification," *IFAC-PapersOnLine*, vol. 56, no. 2, pp. 11369–11376, 2023.
- [36] Z. Zeng, Z. Yue, A. Mauroy, J. Gonçalves, and Y. Yuan, "A sampling theorem for exact identification of continuous-time nonlinear dynamical systems," *IEEE Transactions on Automatic Control*, 2024.
- [37] Z. Zeng, J. Liu, and Y. Yuan, "A generalized nyquist-shannon sampling theorem using the Koopman operator," *IEEE Transactions on Signal Processing*, 2024.
- [38] Y. Susuki, A. Mauroy, and I. Mezic, "Koopman resolvent: A laplace-domain analysis of nonlinear autonomous dynamical systems," *SIAM Journal on Applied Dynamical Systems*, vol. 20, no. 4, pp. 2013–2036, 2021.
- [39] Y. Meng, R. Zhou, M. Ornik, and J. Liu, "Koopman-based learning of infinitesimal generators without operator logarithm," in *63rd IEEE Conference on Decision and Control (CDC)*, IEEE, 2024.
- [40] A. Pazy, *Semigroups of Linear Operators and Applications to Partial Differential Equations*, vol. 44. Springer Science & Business Media, 2012.
- [41] J. C. Willems, "Dissipative dynamical systems part I: General theory," *Archive for Rational Mechanics and Analysis*, vol. 45, no. 5, pp. 321–351, 1972.
- [42] M. O. Williams, I. G. Kevrekidis, and C. W. Rowley, "A data-driven approximation of the Koopman operator: Extending dynamic mode decomposition," *Journal of Nonlinear Science*, vol. 25, pp. 1307–1346, 2015.
- [43] Y. Meng, H. Li, M. Ornik, and X. Li, "Koopman-based data-driven techniques for adaptive cruise control system identification," in *27th IEEE International Conference on Intelligent Transportation Systems (ITSC)*, IEEE, 2024.
- [44] M. Axenides and E. Floratos, "Scaling properties of the Lorenz system and dissipative Nambu mechanics," in *Chaos, Information Processing And Paradoxical Games: The Legacy Of John S Nicolis*, pp. 27–41, World Scientific, 2015.
- [45] S. Sato, M. Sano, and Y. Sawada, "Practical methods of measuring the generalized dimension and the largest lyapunov exponent in high dimensional chaotic systems," *Progress of theoretical physics*, vol. 77, no. 1, pp. 1–5, 1987.
- [46] E. N. Lorenz, "Predictability: A problem partly solved," in *Seminar on Predictability*, vol. 1, Reading, 1996.
- [47] O. Azencot, N. B. Erichson, V. Lin, and M. Mahoney, "Forecasting sequential data using consistent koopman autoencoders," in *International Conference on Machine Learning*, pp. 475–485, PMLR, 2020.
- [48] T. De Ryck, S. Lanthaler, and S. Mishra, "On the approximation of functions by tanh neural networks," *Neural Networks*, vol. 143, pp. 732–750, 2021.
- [49] J. Liu, Y. Meng, M. Fitzsimmons, and R. Zhou, "Physics-informed neural network Lyapunov functions: PDE characterization, learning, and verification," *arXiv preprint arXiv:2312.09131*, 2023.
- [50] F. Camilli, L. Grüne, and F. Wirth, "A generalization of Zubov's method to perturbed systems," *SIAM Journal on Control and Optimization*, vol. 40, no. 2, pp. 496–515, 2001.
- [51] J. Liu, Y. Meng, M. Fitzsimmons, and R. Zhou, "Tool LyZNet: A lightweight Python tool for learning and verifying neural Lyapunov functions and regions of attraction," in *27th ACM International Conference on Hybrid Systems: Computation and Control*, pp. 1–8, 2024.
- [52] R. Zhou, M. Fitzsimmons, Y. Meng, and J. Liu, "Physics-informed extreme learning machine Lyapunov functions," *IEEE Control Systems Letters*, 2024.